ADVANCED MATERIALS
www.advmat.de

Advances in Solution-Processed Multijunction Organic Solar Cells

*Dario Di Carlo Rasi and René A. J. Janssen**

The efficiency of organic solar cells can benefit from multijunction device architectures, in which energy losses are substantially reduced. Herein, recent developments in the field of solution-processed multijunction organic solar cells are described. Recently, various strategies have been investigated and implemented to improve the performance of these devices. Next to developing new materials and processing methods for the photoactive and interconnecting layers, specific layers or stacks are designed to increase light absorption and improve the photocurrent by utilizing optical interference effects. These activities have resulted in power conversion efficiencies that approach those of modern thin film photovoltaic technologies. Multijunction cells require more elaborate and intricate characterization procedures to establish their efficiency correctly and a critical view on the results and new insights in this matter are discussed. Application of multijunction cells in photoelectrochemical water splitting and upscaling toward a commercial technology is briefly addressed.

1. Introduction

Power conversion efficiencies (PCE) of solution-processed organic photovoltaic (OPV) cells have recently reached 14% for single-layer bulk-heterojunctions.[1–3] Crucial to this advancement are the design and optimization of new organic semiconductors and controlling their structural, morphological, optical, and electronic properties. New device architectures, employing selective transport layers for electrons and holes, or optimizing light absorption via advanced light management likewise contributed to the increased PCEs. With PCEs approaching 15%, single-junction OPV cells are closing the gap with thin film photovoltaic technologies based on inorganic and hybrid semiconductors, but still far away from the detailed-balance limit of 33.8% in AM1.5G light.[4,5]

D. Di Carlo Rasi, Prof. R. A. J. Janssen
Molecular Materials and Nanosystems and Institute for Complex Molecular Systems
Eindhoven University of Technology
P.O. Box 513, 5600 MB Eindhoven, The Netherlands
E-mail: r.a.j.janssen@tue.nl
Prof. R. A. J. Janssen
Dutch Institute for Fundamental Energy Research
De Zaale 20, 5612 AJ Eindhoven, The Netherlands
The ORCID identification number(s) for the author(s) of this article can be found under https://doi.org/10.1002/adma.201806499.

DOI: 10.1002/adma.201806499

Single-junction solar cells are principally limited in performance by two factors (**Figure 1**a). Electrons excited by photons with energy higher than the bandgap relax to the band edges, releasing surplus energy as heat (thermalization loss). Photons with energy lower than the bandgap are not absorbed (transmission loss). These losses can be alleviated with two or more absorber layers. The first layer should feature a wide bandgap material to reduce the thermalization loss for high-energy photons. The second layer should have a lower bandgap to absorb the low-energy photons that pass the first layer. In such configuration a tandem cell provides less thermalization and less transmission losses than each of the corresponding single-junction cells. In the detailed-balance limit, a double-junction (tandem) cell can reach an efficiency of 42% and a triple-junction cell 49%.[6]

To construct a tandem cell, the two complementary absorber layers must be stacked optically and electrically (Figure 1b). The interconnecting layer (ICL) between the two subcells must pass light and sustain the photocurrent by providing an optically transparent electrical contact for recombination of electrons and holes from the adjacent photoactive layers. The Fermi level of the hole-transporting layer (HTL) and the electron-transporting layer (ETL) that jointly form the ICL must match the relevant highest occupied molecular orbital (HOMO) and lowest unoccupied molecular orbital (LUMO) levels in the adjacent photoactive layers (Figure 1b). The ICL should not cause voltage losses and have low resistance. The open-circuit voltage (V_{OC}) of the tandem solar cell is ideally the sum of the V_{OC}s of the subcells and the photocurrent is limited by the subcell generating less current. To overcome the intrinsic performance limits of single-junction cells, the subcells should absorb complementary regions of the solar spectrum and generate equal photocurrent.

In the first organic tandem solar cells, materials were thermally evaporated. Initially only metal clusters were used to interconnect the subcells,[7–9] later complemented by p- and n-doped organic transport layers.[10,11] In 2007, the first fully solution-processed tandem polymer solar cells were reported by Gilot et al.[12] and Kim et al.[13] In both examples the ICL featured a layer of poly(3,4-ethylenedioxythiophene):polystyrene sulfonate (PEDOT:PSS) as HTL, stacked on top of either a zinc oxide or a titanium oxide layer as ETL. Kim et al. achieved a PCE of 6.5%. Since then PCEs have steadily increased. Major improvements involved the use of more efficient photoactive blends that afford a high V_{OC} relative to their optical bandgap

E_g.[14] Further, the development of low bandgap absorbers paved the way toward tandems with efficiencies of 8.6% in 2012[15] and 10.6% in 2013.[16] As an alternative to the initially developed conventional structure, inverted tandem solar cells were introduced in which the polarity of the cell was reversed.[17] Also fully organic ICLs were introduced. These alleviated the use and disadvantages of metal oxides. First, partially ethoxylated polyethylenimine (PEIE) was shown to lower the work function of PEDOT:PSS and turn a PEDOT:PSS/PEIE layer into an efficient ICL.[18] Similarly, conjugated polyelectrolytes (CPEs) have recently been used for this purpose.[19] Extending the tandem configuration, multijunction cells with three or more absorber layers have been demonstrated by thermal evaporation[8] and solution-processing[12,20] and with up to 10[21] or 6[22] active layers. Triple-junction devices moved progressively forward, reaching an outstanding PCE of 13.2% for evaporated cells.[23] In 2013, solution-processed triple-junction cells with a PCE of 5.3% were reported by Esiner et al.[24] and with a PCE of 9.6% by Li et al.[25] These triple cells featured a wide bandgap absorber in the front cell and the same small bandgap absorber in the middle and back subcells. In 2014, Chen et al. reported a PCE of 11.6% for a triple-junction cell featuring three complementary bandgaps.[26]

Herein, we discuss recent developments in the field of solution-processed organic tandem solar cells. Because the topic was last extensively reviewed up to 2015,[27–34] we focus on the most salient results obtained since then. In the first part of the review on tandem solar cells, we cover the development and processing of new interconnecting layers, light-management structures, and new photoactive materials for subcells. An overview of the relevant features of the tandem cells published in the covered period is collected in **Table 1**. In the second part, we discuss multijunction cells with three or more active layers, as summarized in **Table 2**. Subsequently pitfalls, intricacies, and protocols for accurate efficiency determination are reviewed. In the last section, we address the use of multijunction organic solar cells for photoelectrochemical and artificial retina applications. General considerations and an outlook complete the review.

Dario Di Carlo Rasi is a Ph.D. student at the Eindhoven University of Technology (TU/e), The Netherlands. He holds a master's degree in materials science and engineering from the University of Rome Tor Vergata, Italy, and made research visits to the University of Wuppertal and Friedrich-Alexander University in Erlangen, Germany. His research involves the design, fabrication, and characterization of multijunction organic solar cells.

René A. J. Janssen is a professor of chemistry and physics at TU/e, The Netherlands. His current research focuses on molecular organic and hybrid semiconductors for optoelectronic applications, energy conversion and energy storage. The work combines synthetic chemistry with optical spectroscopy, morphological characterization and the design, and fabrication and characterization of functional devices.

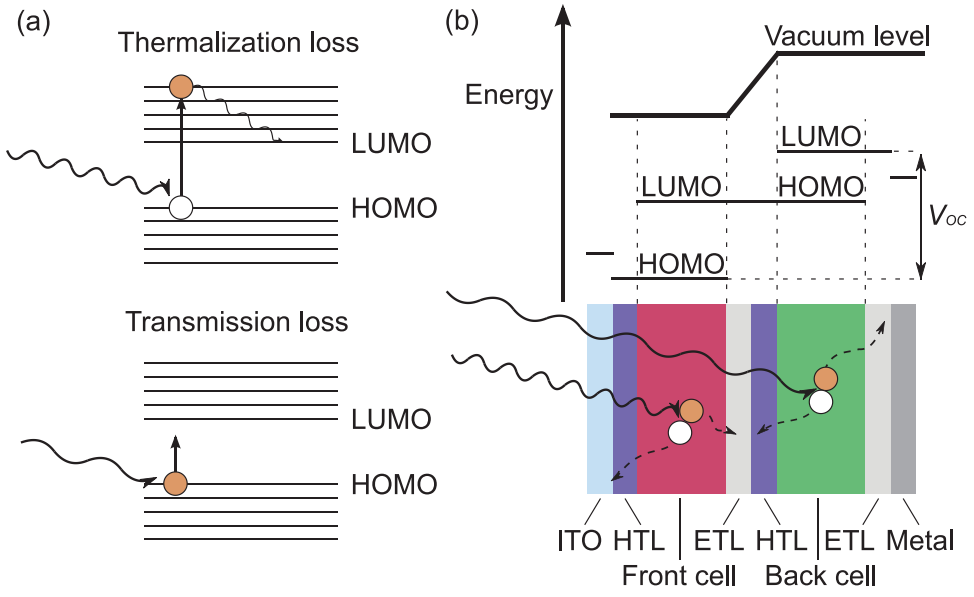

Figure 1. a) Thermalization and transmission losses. b) Arrangement of functional layers and energy levels in an organic tandem solar cell. The ETL/HTL stack between the subcells forms the interconnecting layer.

Table 1. Overview of the relevant data concerning solution-processed organic tandem solar cells covered by the review.

Front subcell			Back subcell			Tandem		Interconnecting layer		Ref.
Material	E_g[a)] [eV]	V_{OC} [V]	Material	E_g[a)] [eV]	V_{OC} [V]	Type[b)]	PCE [%]	Contact to front subcell	Contact to back subcell	
PTB7-Th:$PC_{70}BM$	1.58	0.78	PTB7-Th:$PC_{70}BM$	1.58	0.78	C	11.3	ZnO np	CPEPh-Na	[35]
DR3TSBDT:$PC_{70}BM$	1.74	0.90	DPPEZnP-TBO:$PC_{60}BM$	1.37	0.73	C	12.5	ZnO np	pH–neutral PEDOT:PSS	[104]
PBDB-T:ITCC-M	1.68	1.00	PBDTTT-E-T:IEICO	1.34	0.82	C	13.8	ZnO np	PCP-Na	[36]
PDCBT:$PC_{70}BM$	1.90	0.80	PBDT-TS1:$PC_{60}BM$	1.51	0.80	I	10.2	MoO_3/Ag	ZnO np/PFN	[83]
GEN-2:PCBM	1.76	0.78	PTB7-Th:$PC_{70}BM$	1.58	0.78	I	10.0	PEDOT:PSS(HIL3.3)	ZnO np/PEI	[107]
PBDD4T-2F:$PC_{60}BM$	1.78	0.90	PDPP4T-2F:$PC_{70}BM$	1.37	0.79	I	11.6	MoO_3/Ag	PFN	[84]
PThBDTP:$PC_{70}BM$	1.86	0.95	DPPEZnP-TEH:$PC_{60}BM$	1.37	0.78	C	11.4	PF3N-2TNDI/Ag	PEDOT:PSS	[38]
PIDT-PhanQ:$PC_{70}BM$	1.67	0.86	PTB7:$PC_{70}BM$	1.61	0.73	I	11.0	MoO_3/Ag	PFN	[41]
PTB7-Th:$PC_{70}BM$	1.58	0.79	PTB7-Th:$PC_{70}BM$	1.58	0.79	I	10.8	PEDOT:PSS(PH1000,surfactant)	PEI	[62]
BDT–FBT–2T:$PC_{70}BM$	1.72	0.84	PMDPP3T:$PC_{60}BM$	1.30	0.61	C	8.9	ZnO np	pH–neutral PEDOT:PSS	[86]
P3HT:$PC_{60}BM$	1.90	0.58	PDPP5T-2:$PC_{70}BM$	1.46	0.56	I	4.4	PEDOT:PSS	ZnO np\$Ba(OH)_2$	[116]
PBDTS-TDZ:ITIC	2.09	1.10	PBDTS-TDZ:ITIC	2.09	1.10	I	13.4	PEDOT:PSS/Ag	ZnO np	[101]
P3HT:SF$(DPPB)_4$	1.77	1.11	PTB7-Th:IEIC	1.50	0.95	I	8.5	MoO_3/Ag	PFN	[94]
GEN-2:$PC_{60}BM$	1.75	0.75	PDPP5T-2:$PC_{60}BM$	1.46	0.56	C	6.5	ZnO np	pH–neutral PEDOT:PSS	[112]
PBDD4T-2F:$PC_{70}BM$	1.78	0.90	PBDTTT-E-T:IEICO	1.34	0.81	C	12.8	ZnO np	PCP-Na	[96]
SMPV1:$PC_{70}BM$	1.63	0.88	PTTBDT-FTT:$PC_{70}BM$	1.55	0.74	C	8.5	ZnO	PEDOT:PSS	[113]
P3HT:ICBA	1.90	0.77	PTB7-Th:$PC_{70}BM$	1.58	0.77	I	9.0	PEDOT:PSS(Al4083:PH1000)	PEIE	[115]
DR3TSBDT:$PC_{70}BM$	1.74	0.91	PTB7-Th:$PC_{70}BM$	1.58	0.80	C	11.5	ZnO np	pH–neutral PEDOT:PSS	[81]
PIDTBTO-TT:$PC_{70}BM$	1.87	0.91	PTB7-Th:$PC_{70}BM$	1.58	0.80	C	11.2	PDIN:PFN/Al	MoO_3	[82]
P3TEA:SF-PDI_2	1.72	1.11	P3TEA:SF-PDI_2	1.72	1.11	I	10.8	PEDOT:PSS (HTL)	ZnO sol–gel	[65]
P3HT:$PC_{60}BM$	1.90	0.60	P3HT:$PC_{60}BM$	1.90	0.60	I	3.6	PEDOT:PSS(CPP105D)	AZO sol–gel/PEIE	[49]
P3HT:ICBA	1.90	0.85	PTB7:$PC_{70}BM$	1.61	0.75	I	9.9	$(NH_4)_6P_2Mo_{18}O_{62}$	ZnO np	[57]
P3HT:ICBA	1.90	0.83	PSBTBT:$PC_{70}BM$	1.50	0.63	I	9.3	PEDOT:PSS(surfactant)	TBAI-doped C-$PCBN_3$	[58]
P2F-DO:N2200	1.45	0.80	P2F-DO:N2200	1.45	0.80	I	6.7	PEDOT:PSS(PH500 mod)	ZnO np	[105]
PBDTTT-C-T:$PC_{70}BM$	1.58	0.77	PBDTTT-C-T:$PC_{70}BM$	1.58	0.77	I	8.1	MoO_3 bronze/PF6N25Py	TiO_2 np	[43]
PBDB-T:ITIC	1.59	0.92	PTB7-Th:4TIC	1.40	0.78	I	12.6	MoO_3/Ag	PFN	[95]
P3HT:ICBA	1.90	0.83	BDTT-$(DPP)_2$-CF_3: $PC_{70}BM$	1.55	0.70	I	8.3	PEDOT:PSS(surfactant)	PEIE	[103]
PBDTTPD:$PC_{70}BM$	1.85	0.92	PBDTTPD:$PC_{70}BM$	1.85	0.92	C	8.4	ZnO np/Al	MoO_3	[128]
PTB7:$PC_{70}BM$	1.61	0.73	PTB7:$PC_{70}BM$	1.61	0.73	I	8.1	PEDOT:PSS(HTL mod)	ZnO np	[135]
PTB7:$PC_{70}BM$	1.61	0.74	PTB7:$PC_{70}BM$	1.61	0.72	I	8.2	MoO_3/Ag	PFN	[42]
PTB7-Th:4TIC	1.40	0.76	PTB7-Th:4TIC	1.40	0.76	I/P	11.1	PEDOT:PSS/Ag	Au/MoO_3	[73]
PTZ1:$PC_{70}BM$	1.97	0.94	PBDTTT-C-T:$PC_{70}BM$	1.58	0.74	I	10.3	MoO_3/Ag	PFN	[87]
P3HT:ICBA	1.90	0.84	PBDTTT-C-T:$PC_{70}BM$	1.58	0.77	I	8.2	PEDOT:PSS(surfactant)	a-Zr(acac)/PF6N25Py	[53]

Table 1. Continued.

Front subcell			Back subcell			Tandem		Interconnecting layer		Ref.
Material	E_g[a)] [eV]	V_{OC} [V]	Material	E_g[a)] [eV]	V_{OC} [V]	Type[b)]	PCE [%]	Contact to front subcell	Contact to back subcell	
P3HT:ICBA	1.90	0.69	PCDTBT:$PC_{70}BM$	1.88	0.79	I	7.4	PEDOT:PSS	TSCuPc:SWNTs/TSCuPc	[60]
P3HT:ICBA	1.90	0.79	P3HT:ICBA	1.90	0.83	I	3.6	PEDOT:PSS(PH1000)	PEI	[114]
P3HT:ICBA	1.90	n.a.[c)]	PTB7-Th:$PC_{60}BM$	1.58	n.a.[c)]	I	7.7	PEDOT:PSS(Al4083:PH1000)	PEI	[109]
PTB7-Th:$PC_{70}BM$	1.58	0.77	PTB7-Th:$PC_{70}BM$	1.58	0.77	C	10.2	ZnO np	PEDOT-SO_3Na/p-PFP-O	[37]
PTB7-Th:$PC_{70}BM$	1.58	0.76	PTB7-Th:$PC_{70}BM$	1.58	0.76	I	9.1	PEDOT:PSS(surfactant)	PEI	[63]
PIDTT-DFQT:$PC_{70}BM$	n.a.[c)]	0.91	PCPDT-FBT:$PC_{70}BM$	1.44	0.74	C/T	7.4	C_{60}-SAM/ZnO sol–gel	PEDOT:PSS(PH1000/mod)	[75]
PBDTT-DPP:$PC_{60}BM$	1.44	0.73	TAPC:C_{70}	1.66	0.84	I/P	5.6	MoO_3/Ag	MoO_3	[72]
PThBDTP:$PC_{70}BM$	1.86	0.92	PTB7-Th:$PC_{60}BM$	1.58	0.78	I	8.7	PEDOT:PSS:MoO_3 np	ZnO np/PEI	[50]
HBG1:$PC_{60}BM$	1.80	0.77	PMDPP3T:$PC_{60}BM$	1.30	0.58	I	7.8	PEDOT:PSS(surfactant)	ZnO np	[66]
P3HT:ICBA	1.90	0.77	PTB7:$PC_{70}BM$	1.61	0.71	I	9.9	PEDOT:PSS/Ag nanowires	ZnO np	[52]
PCDTBT:$PC_{70}BM$	1.88	0.88	PSBTBT:$PC_{70}BM$	1.45	0.63	C	6.9	ZnO np	pH–neutral PEDOT:PSS\Nafion	[108]
PTPTIBDT-OD:$PC_{70}BM$	2.04	0.90	PTPTIBDT-OD:$PC_{70}BM$	2.04	0.90	C	5.3	ZnO np	pH–neutral PEDOT:PSS\MoO_3	[138]
PCDTBT:$PC_{70}BM$	1.88	0.88	PBDTT-DPP:$PC_{70}BM$	1.44	0.74	I	9.0	PEDOT:PSS:GO	LZO sol–gel	[59]
PTB7:$PC_{70}BM$	1.61	0.70	PTB7:$PC_{70}BM$	1.61	0.73	I/4T	6.1	ZnO sol–gel	ZnO sol–gel	[74]
PTB7-Th:$PC_{70}BM$	1.58	0.78	PTB7-Th:$PC_{70}BM$	1.58	0.78	I	8.1	MoO_3/Ag	TIPD	[55]
P1:$PC_{70}BM$	1.82	0.91	PTB7-Th:$PC_{70}BM$	1.58	0.81	C	11.4	ZnO np	pH–neutral PEDOT:PSS	[88]
PTB7:$PC_{70}BM$	1.61	n.a.[c)]	PTB7:$PC_{70}BM$	1.61	n.a.[c)]	I	7.0	PEDOT:PSS(FHC/HTL mod)	ZnO np	[77]
P3HT:ICBA	1.90	0.86	PTB7-Th:$PC_{70}BM$	1.58	0.77	I	8.3	PEDOT:PSS(Al4083:PH1000)	PEIE	[79]
PCDTBT:$PC_{70}BM$	1.88	0.88	P(T3-il)-2:$PC_{70}BM$	1.60	0.74	C	6.0	Cr	MoO_3	[45]
P3HT:$PC_{60}BM$	1.90	0.59	P3HT:$PC_{60}BM$	1.90	0.59	C	2.9	TiO_2 sol–gel	PEDOT:PSS:Ag np	[51]
PBDB-T:$PC_{70}BM$	1.80	0.80	PTB7-Th:IEICO-4F	1.24	0.71	I	9.7	MoO_3/Ag	PFN-Br	[98]
DTDCPB:C_{70}	1.68	0.90	PTB7-Th:BT-CIC	1.38	0.69	C	15.0	BPhen:C_{60}/Ag	PEDOT:PSS	[71]
PCDTBT:$PC_{70}BM$	1.88	0.85	PDPP3T:$PC_{60}BM$	1.33	0.63	I	8.0	MoO_3	SnO_x (ALD)	[46]
PTB7:$PC_{70}BM$	1.61	0.72	PDPP4T-2F:$PC_{70}BM$	1.37	0.76	I	10.3	PMA/pH–neutral PEDOT:PSS(mod)	ZnO np	[56]
PTB7:$PC_{70}BM$	1.61	0.75	PDPP4T-2F:$PC_{70}BM$	1.37	0.76	C	10.5	ZnO np	pH–neutral PEDOT:PSS(mod)/PMA	[56]
PBDTTBO:$PC_{70}BM$	1.80	0.86	PDTP-DFBT:$PC_{70}BM$	1.30	0.66	I	10.1	MoO_3/PEDOT:PSS(mod)	Zr-acac	[54]
PSTzBI-EHp:$PC_{70}BM$	n.a.[c)]	0.93	PBDTTT-E-T:IEICO	1.34	0.82	C	12.6	PF3N-2TNDI:PEI	PEDOT:PSS	[39]
PTB7:$PC_{70}BM$	1.61	0.74	PTB7:$PC_{70}BM$	1.61	0.74	I	7.4	PEDOT(CPP105D/HTL mod)	ZnO np	[110]
PBDB-T:F-M	1.65	0.98	PTB7-Th:NOBDT	1.39	0.77	C	14.1	ZnO np	pH–neutral PEDOT:PSS	[99]
PTB7-Th:$PC_{70}BM$	1.58	0.77	PTB7-Th:$PC_{70}BM$	1.58	0.77	I	12.1	PEDOT:PSS(surfactant)	CQD:PEI	[61]
PTB7-Th:$PC_{70}BM$	1.58	0.78	PTB7-Th:$PC_{70}BM$	1.58	0.78	C	9.5	ZnO np	pH–neutral PEDOT:PSS	[76]
PCDTBT:$PC_{60}BM$	1.88	0.90	PDPP5T-2:$PC_{70}BM$	1.46	0.55	I	3.5	MoO_3/PEDOT:PSS	PEI	[137]

Table 1. Continued.

Front subcell			Back subcell			Tandem		Interconnecting layer		Ref.
Material	E_g [a] [eV]	V_{OC} [V]	Material	E_g [a] [eV]	V_{OC} [V]	Type[b]	PCE [%]	Contact to front subcell	Contact to back subcell	
TAPC:C_{70}	1.66	0.89	PCPDTBT:$PC_{70}BM$	1.38	0.59	C	6.3	PTCBI:C_{70}/PTCBI/Ag	HAT-CN	[69]
J52-2F:IT-M	1.60	0.95	PTB7-Th:IEICO-4F	1.24	0.71	C	14.9	ZnO np	PCP-Na	[97]
PBDB-T:F-M	1.65	0.94	PTB7-Th:O6T-4F: $PC_{70}BM$	1.26	0.69	I	17.4	PEDOT:PSS(surfactant)	ZnO np	[102]
PBDB-T:YIT1-2F	1.64	0.93	PTB7-Th:ATT-2	1.32	0.72	C	11.9	ZnO np	pH–neutral PEDOT:PSS	[100]
PTP8:P(NDI2HD-T)	1.80	0.97	PBFSF:N2200	1.45	0.82	I	8.3	MoO_3/Ag	ZnO np	[106]
P3HT:$PC_{60}BM$	1.90	0.60	PCPDTBT:$PC_{70}BM$	1.38	0.60	C	5.7	BCP:Ag/Ag	HAT-CN	[70]
PTzBI-Si:N2200	1.45	0.86	PTzBI-Si:N2200	1.45	0.86	C	11.2	PF3N-2TNDI:PEI	PEDOT:PSS	[40]
PTB7-Th:$PC_{70}BM$	1.58	0.79	PMDPP3T:$PC_{60}BM$	1.30	0.61	I	8.7	PEDOT:PSS	ZnO np	[67]
J71:ITIC	1.59	0.93	PMDPP3T:$PC_{60}BM$	1.30	0.60	C	10.2	SnO_2 np	PEDOT:PSS	[48]
J71:ITIC	1.59	0.92	PMDPP3T:$PC_{60}BM$	1.30	0.61	I	10.4	PEDOT:PSS	SnO_2 np	[48]
PDPP3T:$PC_{60}BM$	1.33	0.67	PDPP3T:$PC_{60}BM$	1.33	0.67	I	5.6	PEDOT:PSS	PEIE	[139]

[a] E_g is the lowest optical bandgap of the materials blended in the active layer, with exception of fullerene derivatives, for which it was omitted; [b] C: conventional structure; I: inverted structure; P: parallel connection; 4T: four-terminal connection; T: illuminated from the top; [c] Not available.

2. Tandem Solar Cells

2.1. Interconnecting Layer Materials

The materials forming the ICL are key to the optimal performance of tandem cells. The ICL connects the subcells, optically and electrically, preferably without losses. Optical transparency, uniformity, mechanical robustness, solvent orthogonality during processing, matching with the relevant HOMO and LUMO levels and Ohmic character are important requisites. The ICL often consists of combinations of polymeric and metal oxide materials. PEDOT:PSS as HTL and zinc oxide nanoparticles as ETL remain a widely adopted combination of materials. From Table 1, it emerges that also evaporated molybdenum oxide as HTL, followed by a thin (discontinuous) layer of silver and poly[(9,9-bis(3′-(*N*,*N*-dimethylamino)propyl)-2,7-fluorene)-alt-2,7-(9,9-dioctylfluorene)] (PFN) as ETL, is frequently used. Nevertheless, several new materials have been introduced in recent years. Especially, CPEs and structurally related pH–neutral self-doped conductive polymers (SCPs) are a largely explored alternative both for the p- as well as the n-type charge transporting layers. Decorating a conjugated polymer with anionic or cationic side groups can create dipole moments that change the work function of the substrate on which they are coated. The CPEs are often wide bandgap semiconducting materials that serve to change the work function. CPEs and SCPs are often used as thin layers (<25 nm) to reduce parasitic light absorption. Generally, CPEs are processed from alcoholic solvents because these are compatible with most of the tandem stacks. **Figure 2** provides the chemical structure of the materials discussed hereafter.

In 2015, Zhou et al. presented two new CPEs: PCPDTBTSO$_3$K (CPE-K) and PCPDTPhSO$_3$Na (CPEPh-Na).[35] Owing to the ionic side groups, a thin layer (10–15 nm) of these p-type materials could effectively increase the work function of the substrate to 5.2 eV. Tandem devices using a zinc oxide nanoparticles layer coated with CPEPh-Na as ICL showed a PCE up to 11.3%. Structurally similar is the p-type CPE PCP-Na, adopted by Cui et al.[36] An ICL of zinc oxide nanoparticles and PCP-Na allowed the realization of over 13% PCE in tandems with state-of-the-art photoactive materials. An interesting CPE in this series is p-PFP-O, used in a tandem device by Lee et al.[37] p-PFP-O derives from the oxidative doping of its n-type counterpart (PFP-O), by treating the latter with ammonium persulfate. As a consequence of the oxidation, the orientation of the dipole moment is reversed, with respect to PFP-O. The authors successfully demonstrated the good performance (PCE ≈10%) of this CPE in a tandem cell with a zinc oxide/PEDOT-SO$_3$Na/p-PFP-O ICL, where PEDOT-SO$_3$Na is a pH–neutral form of PEDOT. pH–neutral PEDOT has a low work function and to avoid loss in V_{OC}, the p-PFP-O was used. Zhang et al. presented PF3N-2TNDI as a useful CPE for the n-type side of an ICL in combination with PEDOT:PSS on the p-side and an ultrathin silver layer in between.[38] The role of silver is to provide a recombination center for charges from the subcells. PF3N-2TNDI could reduce the work function of silver down to 4.1 eV. The CPE proposed by Zhang et al. outperformed the well-known PFN, not only in terms of PCE but also as reduced dependence of the performance on its thickness (PCE still 9.7%

Table 2. Overview of the relevant data concerning solution-processed organic triple- and quadruple-junction solar cells.

Cell configuration[a)]	E_g[b)] [eV]	V_{OC} [V]	Type[c)]	PCE [%]	Interconnecting layer front | back	Ref.
PSEHTT:ICBA (1) PTB7:PC_{70}BM (2) PMDPP3T:PC_{70}BM (3)	1.82 1.61 1.30	2.24	Threefold I	11.8	pH–neutral PEDOT:PSS | LZO sol–gel/C_{60}-SAM	[127]
PCDTBT:PC_{70}BM (1) PMDPP3T:PC_{60}BM (2,3)	1.88 1.30	2.03	Threefold C	6.7	ZnO np | pH–neutral PEDOT:PSS	[129]
PBDTTPD:PC_{70}BM (1–3)	1.85	2.75	Threefold C	7.4	ZnO np | Al/MoO_3	[128]
PTB7:PC_{70}BM (1–3)	1.61	2.13	Threefold I	8.7	MoO_3/Ag | PFN	[130]
PCDTBT:PC_{70}BM (1) PDPPTPT:PC_{60}BM (2) PDPP5T:PC_{60}BM (3)	1.88 1.53 1.46	2.26	Threefold I	6.0	PEDOT:PSS | ZnO np	[67]
PDCBT:PC_{60}BM (1) PDPPTPT:PC_{70}BM (2) PMDPP3T:PC_{60}BM (3)	1.90 1.53 1.30	2.20	Threefold I	8.7	PEDOT:PSS | ZnO np	[67]
PDCBT:PC_{60}BM (1) PTB7-Th:PC_{70}BM (2) PMDPP3T:PC_{60}BM (3)	1.90 1.58 1.30	2.15	Threefold I	10.0	PEDOT:PSS | ZnO np	[67]
PDCBT:PC_{60}BM (1) PTB7-Th:PC_{70}BM (2) PMDPP3T:PC_{60}BM (3) PDPPSDTPS:PC_{60}BM (4)	1.90 1.58 1.30 1.13	2.45	4-fold I	7.6	PEDOT:PSS | ZnO np	[68]
PDPP5T-2:PC_{60}BM (1,2) PCDTBT:PC_{70}BM (3)	1.46 1.88	0.89	Threefold S/P	5.4	ZnO np | pH–neutral PEDOT:PSS	[131][d)]
PDPP5T-2:PC_{60}BM (1,2) OPV12:PC_{60}BM (3)	1.46 1.73	0.82	Threefold S/P	5.4	ZnO np | pH–neutral PEDOT:PSS	[131][d)]

[a)]The numbers in parentheses refer to the subcell number in the stack, with 1) being the front cell; [b)]E_g is the lowest optical bandgap of the materials blended in the active layer, with exception of fullerene derivatives, for which it was omitted; [c)]C: conventional structure; I: inverted structure; S/P: series/parallel triple; [d)]Consult the main text for more details.

at 20 nm). In 2018, the same group demonstrated that by mixing PF3N-2TNDI with polyethyleneimine (PEI), the work function could be further lowered without significantly affecting charge transport.[39,40] With the optimal mixed ETL, a high performing tandem was fabricated without the need of the silver layer in between ETL and PEDOT:PSS. The tandem afforded a PCE of 11%, even at 70 nm thickness of this ETL (the optimal PCE was 12.6% at a thickness of 20 nm).[39] A good performance for tandems adopting PFN was reported independently by Zuo et al.[41] and Martínez-Otero et al.,[42] both in 2015. The ICL used consisted of evaporated molybdenum oxide with an ultrathin layer of silver and PFN on top. PCEs approaching 11%[41] and an extraordinarily high fill factor (FF) of 0.76[42] were achieved. Even with a total thickness below 20 nm,[42] the ICL provided the necessary protection of the front cell from processing of the back cell on top and good optical transparency. Continuing with the n-type CPEs, Lu et al. demonstrated a novel ICL consisting of all solution–processed metal oxide/dipole layer/metal oxide.[43] PF6N25Py was used to make a layer on top of another layer of molybdenum bronze. The work function of the latter was effectively lowered, improving the energy level alignment with a subsequent film of titanium dioxide nanoparticles.[43] By fabricating homo tandems with this ICL, a correct addition of the V_{OC} of the subcells was obtained, together with comparable FF to the single-junction reference cell and improved overall efficiency.

Metal oxides are a very popular class of interlayer materials for electronics in general and for OPV as well. Metal oxides commonly adopted in OPV are deposited either from preformed nanoparticles suspensions, from a metal-organic precursor in solution which converts to some extent to a metal oxide or via thermal evaporation in high vacuum. Examples of all-oxide ICLs are rare and always involve the presence of thin metal clusters to improve their conductivity.[17,44] An example was provided by Bag et al. in 2016, where they used an ICL made of evaporated chromium and molybdenum oxide.[45] Only in 2018, Becker et al. reported the first all-oxide ICL for polymer tandem solar cells.[46] A possible reason for the scarcity of such examples might be because very few metal oxide layers guarantee the protection of the front cell active layer against the processing from solution of the back cell active layer.[38] The exceptional example of Becker et al. consisted of an inverted (n–i–p) configuration tandem in which thermally evaporated molybdenum oxide (HTL) and tin oxide (ETL) deposited via atomic layer deposition were stacked together to form the ICL. A large intrinsic interface dipole at the interface HTL/ETL makes the conduction bands of molybdenum oxide and tin oxide to align. In addition, the tandem featuring this ICL did not suffer from the well-known problem of necessity of UV light soaking. In fact, it is known that exposing common conductive metal suboxides, such as zinc oxide and titanium dioxide, to UV light illumination can increase their conductivity by a photodoping mechanism.[47] In 2018, Di Carlo Rasi et al. used solution-processable tin oxide nanoparticles suspensions for the fabrication of OPV tandems.[48] In combination with PEDOT:PSS as HTL, the tin oxide ETL provides efficient tandem cells in conventional (p–i–n) and inverted (n–i–p) architectures. For conventional tandems, tin oxide offers the possibility to avoid the use of pH–neutral PEDOT:PSS, which can cause a loss in V_{OC} due its reduced work function. In fact, tin oxide proved to be resistant against the acidity of the commercial formulation of PEDOT:PSS (Al 4083), while zinc oxide layers are washed away. Mitul et al. implemented solution-processed aluminum-doped zinc oxide (AZO) in a PEDOT:PSS/AZO/PEIE ICL.[49] Thermal annealing at 150 °C was required to form AZO from its precursor. To demonstrate the proper working of this ICL, the authors built a homo tandem using P3HT:PCBM, which can sustain this temperature. Du et al. reported molybdenum oxide nanoparticles as a solution to overcome interfacial losses occurring in some tandem solar cells where PEDOT:PSS is used as HTL.[50] They attributed poor hole transporting properties of the interface between PEDOT:PSS and an active layer with polymers containing nitrogen atoms to the protonation of the latter. By mixing PEDOT:PSS and

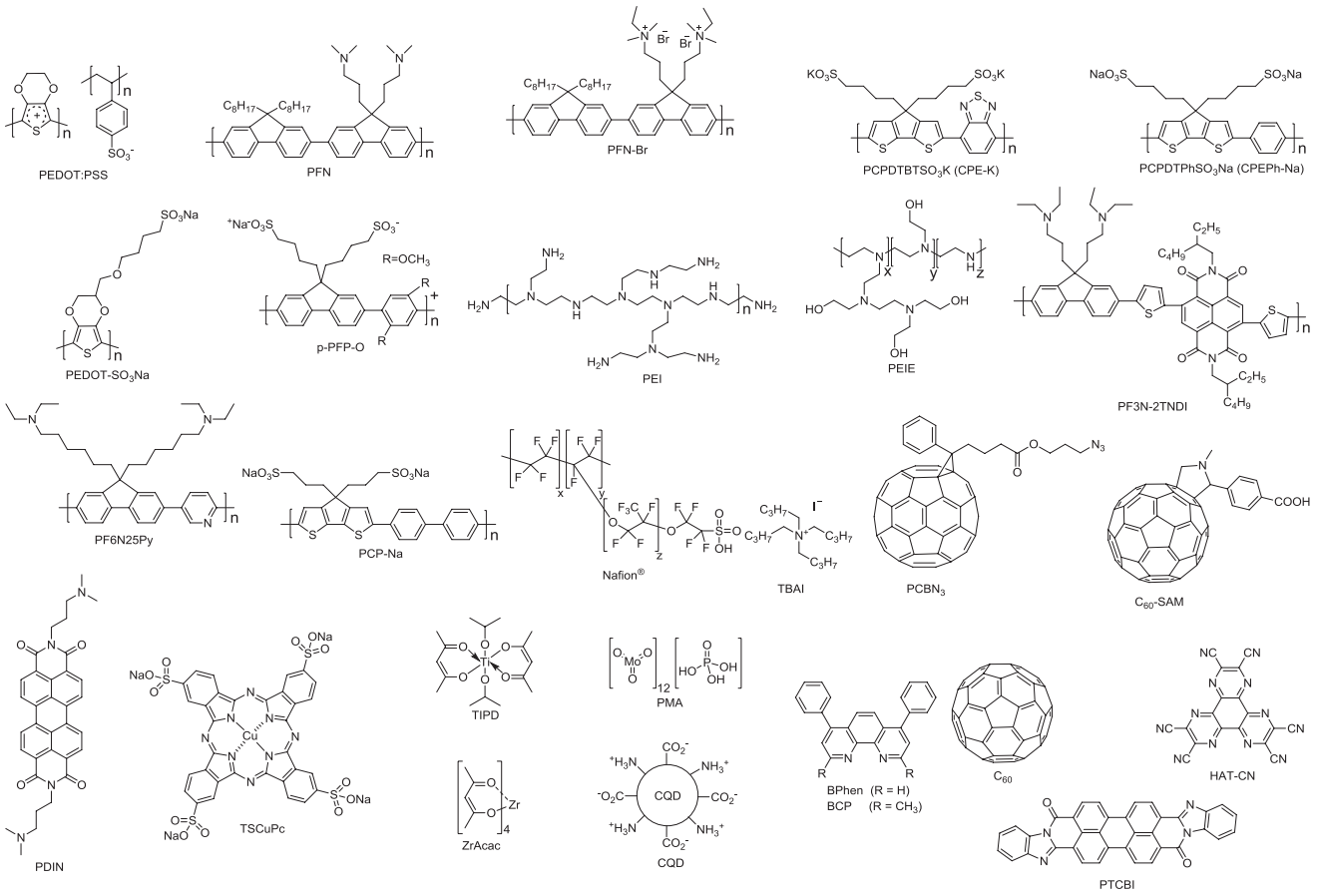

Figure 2. Materials adopted in the ICL of tandem solar cells. The references for publications using these materials are provided in Table 1.

MoO_3 nanoparticles, the problem was reported to be solved and tandem solar cells using a PEDOT:PSS:MoO_3/ZnO/PEI ICL showed improved performance compared to the control tandem devices with only PEDOT:PSS or MoO_3. Torabi et al. reported a mixture of modified PEDOT:PSS and silver nanoparticles as HTL in the ICL, in combination with sol–gel titanium dioxide as ETL.[51] The silver nanoparticles were synthesized directly in the dispersion of the modified PEDOT:PSS by reduction of the silver nitrate precursor with sodium borohydride, without the need of a stabilizer. A homo tandem was fabricated to demonstrate the performance. The V_{OC} was 1.1 V and the FF 0.60, against the 0.59 V and FF of 0.55 of the reference cell. Raïssi et al. describe the use of PEDOT:PSS/Ag nanowires/ZnO nanoparticles as ICL of tandem cells.[52]

Recently, a few examples of tandem solar cells have emerged in which metal-organic compounds have been adopted in the ICL. Lu et al.[53] and Chang et al.[54] adopted zirconium acetylacetonate (Zr-acac) to lower the work function of PEDOT:PSS in the ICLs: PEDOT:PSS/Zr-acac/PF6N25Py and MoO_3/PEDOT:PSS/Zr-acac, respectively. Zr-acac has the advantage that it can easily be processed from solution and does not require a thermal annealing treatment. Another example of metal chelate in tandems was reported by Shi et al.[55] In their work, Shi et al. used titanium (diisopropoxide)bis(2,4-pentanedionate (TIPD) on top of evaporated MoO_3/Ag as ICL, applying a post-treatment of 150 °C to get the optimal performance of the tandem cell. One example of an inorganic transition metal compound for tandem applications is represented by the phosphomolybdic acid hydrate (PMA), presented by Lu et al. in both conventional and inverted structure tandems.[56] In their work, a modified pH–neutral PEDOT:PSS layer served as recombination center for the charges extracted by the PMA HTL and the zinc oxide nanoparticles ETL. The ICL was then PMA/PEDOT:PSS/ZnO in inverted tandem cells and vice versa for the conventional cells. The work function of pH–neutral PEDOT:PSS does not match the deep-lying HOMO energy level of some photoactive polymers, generally provoking a loss in V_{OC}.[24] By using PMA in between pH–neutral PEDOT:PSS and the active layer of P3HT:PC_{60}BM, the authors showed a recovery in the V_{OC} with respect to the control device without PMA (0.62 V vs 0.48 V, respectively). Vasilopoulou et al. adopted an inorganic molecular metal oxide processed from methanol in the ICL of a tandem cell.[57] In particular, a layer of polyoxometalate (POM) was used as HTL, on top of the front cell active layer, followed by ZnO nanoparticles as ETL. The front cell comprised P3HT:ICBA, and the back cell included PTB7:PC_{70}BM. The POM considered for the tandem was $(NH_4)_6P_2Mo_{18}O_{62}$. The authors reported a number of electronic properties of this one, such as a high work function (6.0 eV), very deep HOMO energy (8.2 eV), and deep LUMO energy (5.6 eV). Because of the similarity between the LUMO energy of the POM and the HOMO energy of the electron-donating material in the

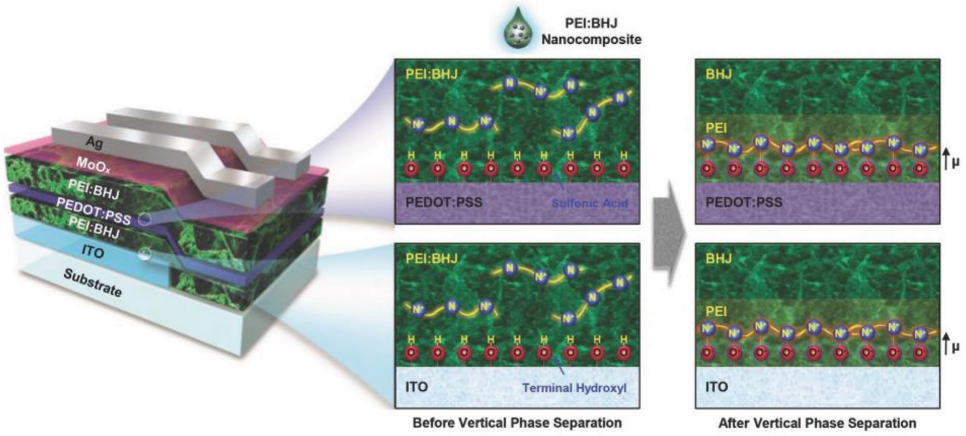

Figure 3. Tandem polymer solar cell processed from bulk heterojunction:PEI nanocomposite solution. Reproduced with permission.[62] Copyright 2014, Wiley-VCH.

front cell (P3HT), they proposed that this LUMO level takes part in the recombination process in the ICL. The characterization of the tandem device revealed a nearly loss-free V_{OC} of 1.59 V (1.60 V expected) and a high FF of 0.69. The measured short-circuit current density (J_{SC}) amounted to 9.05 mA cm^{-2}, although the summed external quantum efficiencies (EQE) of the subcells, approaching 150%, cannot be used to support this value.

Allotropic forms of carbon have also been used in ICL. In 2015 Chang et al. used a cross-linkable azidofullerene derivative ((C-)PCBN$_3$), doped with tetrabutylammonium iodide (TBAI) as ETL, on top of PEDOT:PSS.[58] A temperature of 140 °C was used for the curing of the ETL, which allowed the manufacturing of tandems on a flexible polyethylene naphthalate substrate with good performance (PCE of 8.7% vs 9.3% on glass). The ETL also showed a weak thickness dependence of the performance, with an optimum at 10 nm. A mixture of PEDOT:PSS and graphene oxide has been reported by da Silva et al. to work in an ICL, together with lithium-doped zinc oxide (LZO) as ETL.[59] Raïssi et al. showed an ICL consisting of PEDOT:PSS, on top of which they deposited an ETL made from a mixture of single-walled carbon nanotubes (SWNT) and a phthalocyanine derivative (TSCuPc), and the sole phthalocyanine.[60] Another form of carbon for the ICL is carbon quantum dots (CQDs), mixed with PEI as described by Kang et al.[61] CQDs were synthesized by a microwave reaction starting from citric acid and β-alanine, resulting in particles with a size of ≈3 nm. A thin layer of the CQDs/PEIE composite on top of PEDOT:PSS was reported to provide an efficient tunneling junction for the recombination of charges in the ICL, affording a best efficiency of 12.1%.

2.2. Processing Multijunction Stacks

For a future tandem, OPV technology is important to simplify manufacturing processes. In this section, recent advances focusing on processing of tandem OPV cells are reported.

Lee et al.[37,62,63] adapted a concept first introduced by Wei et al.[64] for single-junction OPV devices to tandem solar cells. The idea is to process both the photoactive components and interlayer material from the same solution. By taking advantage of different surface energy of these components, a favorable spontaneous segregation of the interlayer materials at the desired interfaces can take place during the deposition (**Figure 3**). In their tandem devices, Lee and co-workers mixed either PEI[62,63] or p-PFP-O[37] with the active layer blend materials. For the latter, they choose a widely reported combination: PTB7-Th as electron donor and PC$_{70}$BM as electron acceptor. Inverted[62,63] and conventional[37] tandems were demonstrated using this technique to process both the front and the back subcells, where the ICL was either PEDOT:PSS/PEI[62,63] or zinc oxide/PEDOT-SO$_3$Na/p-PFP-O.[37] Time-of-flight secondary-ion mass spectrometry measurements confirmed the localization of PEI at two positions (bottom and top subcells) along the vertical direction of the stack, rather than being uniformly distributed.

Recent reports focused on the improved processing of PEDOT:PSS/zinc oxide as ICL for inverted tandem solar cells. In 2017, Chen et al. reported the processing of diethyl zinc precursor on top of a "wet" (not annealed) layer of PEDOT:PSS as ICL.[65] According to the authors, the residual moisture in the PEDOT:PSS film promoted the conversion of the precursor to zinc oxide. The as-formed layer of zinc oxide only needed a mild thermal annealing at 80 °C, which was compatible with the front cell active layer. As a result, a record V_{OC} of 2.16 V, combined with a 10.2% efficiency, was achieved in a tandem device. Given the hydrophobic nature of commonly adopted active layer materials, the deposition of a layer of PEDOT:PSS from an aqueous dispersion requires the use of surfactants to lower the surface energy. Surfactants are in general insulating and the amount necessary to improve the casting can eventually be substantial and deteriorate the desired properties of PEDOT:PSS. Moreover, modifying PEDOT:PSS might affect unfavorably the distribution of the insulating PSS part, creating an energy barrier. Prosa et al. proposed a simple approach to recover the good functioning of a PEDOT:PSS film deposited from a suspension including a surfactant (Zonyl FS-300).[66] By simply rinsing the film with isopropanol, part of the surfactant and the excess of PSS at the surface of the layer could be removed. Tandems with isopropanol-rinsed PEDOT:PSS, followed by zinc oxide nanoparticles as ICL, demonstrated

optimal performance, contrary to the pristine device with non-rinsed PEDOT:PSS. In fact, the latter featured an s-shape in the current-density–voltage (*J*–*V*) characteristics, denoting the presence of an interfacial barrier. Di Carlo Rasi et al. demonstrated how both the requirements of a low annealing temperature of the ICL and a low surface energy of the PEDOT:PSS dispersion can be satisfied at the same time.[67] It was found that by processing the commercial formulation of PEDOT:PSS (Al4083) from a mixture of water/1-propanol (1:2 v/v) in inert atmosphere provides a good coverage for a wide selection of different active layer materials, without the need of a surfactant. To complete the ICL, zinc oxide nanoparticles in isoamyl alcohol were spin coated on the PEDOT:PSS layer. Without thermal annealing, the proposed processing technique afforded six tandems and three triple-junction solar cells featuring eight active layer materials of different chemical nature. Using the same technique, the first example of a solution-processed quadruple-junction polymer solar cell with four complementary absorber layers was reported.[68]

Orthogonality of the solutions is a stringent requirement for fabricating complex device stacks such as tandems directly from solution. A possible way to get around this constraint is to stamp transfer the top subcell, avoiding the use of solvents. In 2017, Ka et al. demonstrated an example of device fabricated in this fashion. In their work, they deposited a front cell consisting of the small molecular donor TAPC blended with C_{70}.[69] Next in the stack they deposited, also by thermal evaporation, a PTCBI:C_{70} buffer electron transport layer, preceding a PTCBI/Ag/HAT-CN interconnecting layer. For the back cell they adopted PCPDTBT:$PC_{70}BM$, which has a low bandgap of 1.38 eV. The latter was deposited by spin-coating onto a poly(dimethylsiloxane) stamp, dried in high vacuum from solvents, coated onto the evaporated front subcell/ICL stack, and detached from the stamp after annealing at 100 °C under applied pressure, to form a conformal contact at the interface. The resulting tandem was characterized by a correct addition of the V_{OC} of the subcells: this was 0.89 and 0.59 V for the front and the back subcells respectively, while for the tandem 1.46 V of V_{OC} was measured. Maybe due to the limited FF of both the single-junction cells, the tandem featured an FF of only 0.51, limiting the efficiency to 6.26%. Later, in 2018 Ka et al. also demonstrated a polymer tandem solar cell where both the front and the back subcells were deposited by stamp transfer and the interlayers were obtained by thermal evaporation.[70] P3HT:$PC_{60}BM$ was adopted in the front cell and PCPDTBT:$PC_{70}BM$ as back cell. The tandem showed full addition of the V_{OC} (1.20 V) and an FF of 0.60. In 2018, Che et al. revisited the same concept of combining a thermally evaporated front cell with a solution-processed back cell.[71] Different from the work discussed before, the back subcell was directly deposited by spin-coating on top of the evaporated front subcell. The former was a DTDCPB:C_{70} coevaporated cell, coated with ETL BPhen:C_{60}/Ag, also by thermal evaporation. Following, PEDOT:PSS was cast to complete the ICL, and the back cell of PTB7-Th:BT-CIC was deposited by spin-coating. The front cell donor material has a wide bandgap of 1.68 eV, while donor and acceptors in the back cell have bandgaps of 1.58 and 1.38 eV, respectively. An outstanding high PCE of 15% was obtained by this tandem cell, arising from an EQE between 70% and 80%, corresponding to a measured J_{SC} of 12.7 mA cm^{-2}. By applying an antireflection coating on the glass facade, the J_{SC} increased even further, up to 13.3 mA cm^{-2}. In addition, the V_{OC} of 1.59 V followed the sum of the constituent subcells (0.90 and 0.69 V for the front and back cells, respectively), together with a high FF of 0.71. Another remarkable aspect of this work is the high yield accompanying the high efficiency: 97% and 95% for solar cells with active area of 2 and 9 mm^2, respectively, from a total of 130 devices.

2.3. Light Management

Organic multijunction solar cells feature stacks of several semitransparent thin films. For such devices, optical interference effects play an important role. Hence, a number of papers have focused attention on how to take advantage of these effects, in order to improve the balance of absorption of light from the two subcells. Zuo et al. explored the influence of the thickness of the Ag layer in a MoO_3/Ag/PFN ICL on the balance of current from the subcells.[41] In particular, an optical microcavity is formed between the thin silver layer in the ICL (8–14 nm) and the opaque silver contact on the back cell (**Figure 4**).

By acting on the thickness of the thin silver layer, the balance of absorption between front and back subcells could be tuned to achieve current matching. Moreover, the authors were able to measure the individual subcells directly by accessing externally the intermediate silver contact. A similar phenomenon was observed in tandem cells with parallel connection by Lee et al.[72]

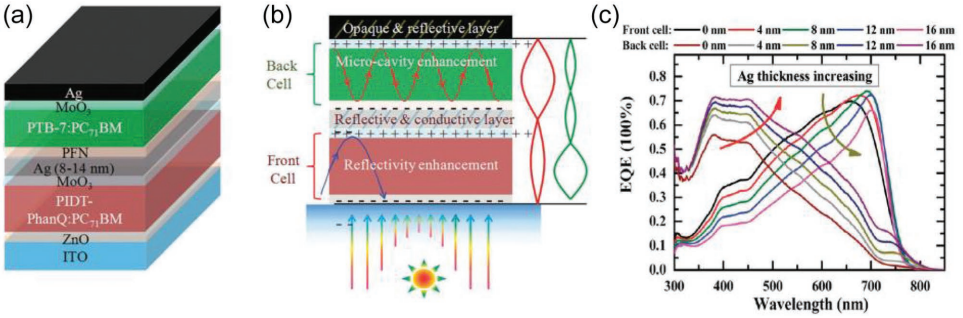

Figure 4. Microcavity tandem polymer solar cell. a) Device scheme. b) Schematic illustrating the microcavity enhancement in the back cell. c) Modeled EQE spectra of the subcells as a function of the thickness of the Ag layer in the ICL. Reproduced with permission.[41] Copyright 2015, The Royal Society of Chemistry.

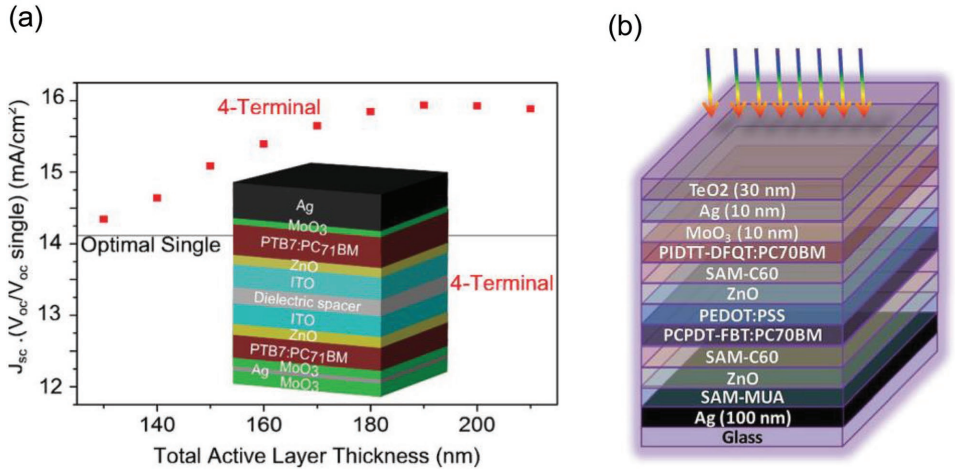

Figure 5. a) Four-terminal tandem. Reproduced with permission.[74] Copyright 2015, American Chemical Society. b) Top-illuminated tandem with DMD electrode. Reproduced with permission.[75] Copyright 2015, The Royal Society of Chemistry.

and Zuo et al.[73] In the first case MoO_3/Ag/MoO_3 was the ICL, while in the second case it was PEDOT:PSS/Ag/Au/MoO_3. In a parallel-connection tandem, the requirement of current matching drops since the total current is the summation of the current of the subcells. Besides the increase in current, the voltage is pinned to the lowest voltage between the two subcells. Due to the limited charge mobility in most of the organic semiconductors, the optimal thickness of a single-junction device is usually determined by the tradeoff between increasing charge generation by more light absorption in thicker layers and the concomitant decrease because of bimolecular charge recombination. To increase light absorption while preserving the fill factor (influenced by charge recombination), the same active layer absorber can be deposited twice in a homo tandem. The one reported by Zuo et al. in particular, represented at the time the most efficient example for organic tandem solar cell with parallel connection (PCE of 11.1%). PTB7-Th:4TIC was used as active layer. Again to improve the absorption of active layers suffering from thickness-dependent performance, Mantilla-Perez et al. fabricated a four-terminal homo-tandem solar cell.[74] A glass substrate coated with indium-doped tin oxide (ITO) on both sides was used to build single-junction cells on each side (**Figure 5**a).

A dielectric–metal–dielectric (DMD) stack was deposited as transparent electrode by thermal evaporation on top of one of the active layers, consisting of MoO_3/Ag/MoO_3. The top electrode on the other subcell was an opaque metal. Another advantage of this special architecture is that the two subcells can be operated independently, which solves the requirement of current or voltage matching. As pointed out by the authors, a limiting factor in their particular device was the DMD electrode due to its poor transparency. Related to this point, Zuo et al. reported a series-connected tandem solar cell featuring a MoO_3/Ag/TeO_2 DMD transparent top electrode.[75] The device was built starting from an opaque silver layer on glass as bottom electrode and finished with the DMD stack on top (Figure 5b). Interestingly, the DMD tandem had a performance close to the ITO-based counterpart, thanks to the TeO_2 capping layer, which reduced the reflection at the thin silver layer, the first one encountered by light. Another way to enhance the absorption of the active layers was reported by Mayer et al.[76] Here, a templated periodical structure was applied externally on the glass side of an ITO-based tandem solar cell. The structure reported was made with a UV-curable polymer on a glass substrate and a master template fabricated with laser interference lithography. A relative increase by 9% in the PCE was recorded following the application of this diffractive structure.

Optical interference in tandem solar cells is usually optimized considering illumination in the direction perpendicular to the surface of the device. Nevertheless, in practical scenarios the solar cell is not constantly oriented in such direction but there is rather a certain angle of incidence. Mertens et al.[77] tried to understand a peculiar behavior of organic tandem solar cells, already reported by Riede et al.[78] for evaporated tandem cells. In detail, when their device was at a certain angle of orientation Θ with respect to the direction of incidence of light, the short-circuit current density corrected for the effective area of illumination ($J^*_{SC} = J_{SC}/\cos(\Theta)$) was relatively insensitive to this angle, up to 65°.[77] In their work, the authors showed that both the measured and modeled EQE spectra of the individual subcells change according to Θ. Nevertheless, both of the corresponding spectrally integrated J^*_{SC}s stay relatively constant. The angle insensitivity of the performance of organic tandem solar cells is particularly interesting for their application in realistic operating conditions.

For building-integrated photovoltaics, color tunability is important. In 2017, Luo et al. reported flexible all solution–processed polymer tandem solar cells with different colors.[79] Owing to a highly conductive PEDOT:PSS top electrode, the reflectivity of the device was engineered by simply changing the thickness. PCE values from 7.23% to 8.34% were achieved, corresponding to different colors.

2.4. Active Layer Materials

In order to exploit the full potential of tandem solar cells, the active layer materials need to be engineered to not only have

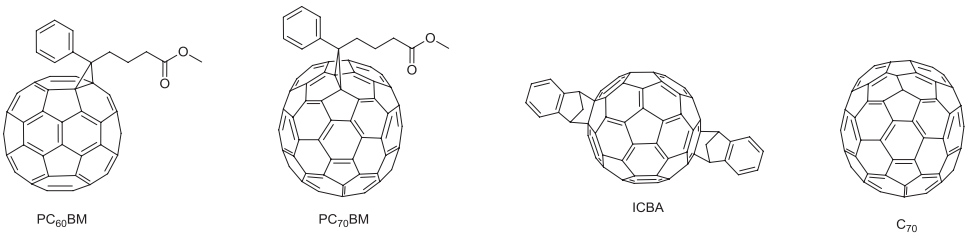

Figure 6. Fullerene acceptors used in tandem solar cells. The references for publications describing these materials are provided in Table 1.

different bandgaps but also absorb light in complementary regions of the solar spectrum such that high energy photons that pass the first layer are not absorbed in the second layer and are reflected at the back electrode. The optimal thickness of single-junction cells is known to be limited by bimolecular recombination, and developing photoactive absorber blends with thickness-insensitive performance, e.g., via the creation of a suitable blend morphology, can alleviate the disadvantages of spectral overlap between the two subcells and increase the photocurrent. To afford a high V_{OC} tandem, both the subcells should possess a low minimum photon energy loss (E_{loss}), defined as $E_{loss} = E_g - eV_{OC}$. A number of materials, either newly developed or previously reported in single-junction devices, have been adopted in tandem solar cells for this purpose. For a complete list of photoactive materials, either small molecules or polymers, and their optical gap, we refer to Table 1. **Figures 6–10** show their chemical structures.

Photoactive blends based on PCBM were traditionally the most diffused and studied. Benefiting from its isotropy, PCBM works reasonably well with a wide range of polymer donors. PTB7-Th represents a benchmark donor material for polymer–fullerene blends in recent years, especially for tandem solar cells. With a bandgap of 1.58 V, a single-junction device based on this material and $PC_{70}BM$ features a V_{OC} around 0.8 V and efficiency up to 10% or more.[80] When blended with $PC_{70}BM$, an efficiency of 11.3% was reported for a homo-tandem device with this active layer despite the lack of complementarity in the absorption due to the use of the same absorber for both the front and back subcells.[35] More groups reported similar efficiencies for tandem cells featuring this blend in one of the two subcells.[61,81,82] Zheng et al. combined the polythiophene PDCBT and the benzodithiophene-based PBDT-TS1, blended with $PC_{70}BM$ and $PC_{60}BM$, respectively in a tandem device.[83] The first one has a wide bandgap of 1.90 eV and the second one has a bandgap of 1.51 eV. Both possessed maximum EQEs around 70% in optimal single-junction devices and V_{OC}s of 0.80 V. The authors fabricated a tandem by using the PDCBT blend for the front cell and the PBDT-TS1 blend as back cell. A PCE of 10.2% was reported for this device. Besides a moderate FF of 0.55, the device showed a correct addition of the V_{OC} of the subcells (V_{OC} = 1.60 V) and a remarkable J_{SC} of 11.7 mA cm^{-2}. This high value of J_{SC} is derived from the EQE spectrum of the subcells, being as high as almost 70% (back cell) and ≈75% (front cell). Nevertheless some concerns arise because the summed EQE of the subcells is over 100% around 450 nm. In 2016, the same group synthesized a new low bandgap polymer[84] by introducing fluorine atoms in the structure of the already reported PDPP4T.[85] Compared to PDPP4T, the fluorinated version PDPP4T-2F showed a slightly broader absorption spectrum, the onset being at ≈900 nm. The main advantage of this new version consists in the high V_{OC} it can give, when mixed with $PC_{60}BM$, thanks to the lower HOMO level (0.12 eV lower). The difference in V_{OC} of the single-junction cells reflected perfectly the difference in HOMO: 0.78 V versus 0.66 V for PDPP4T-2F

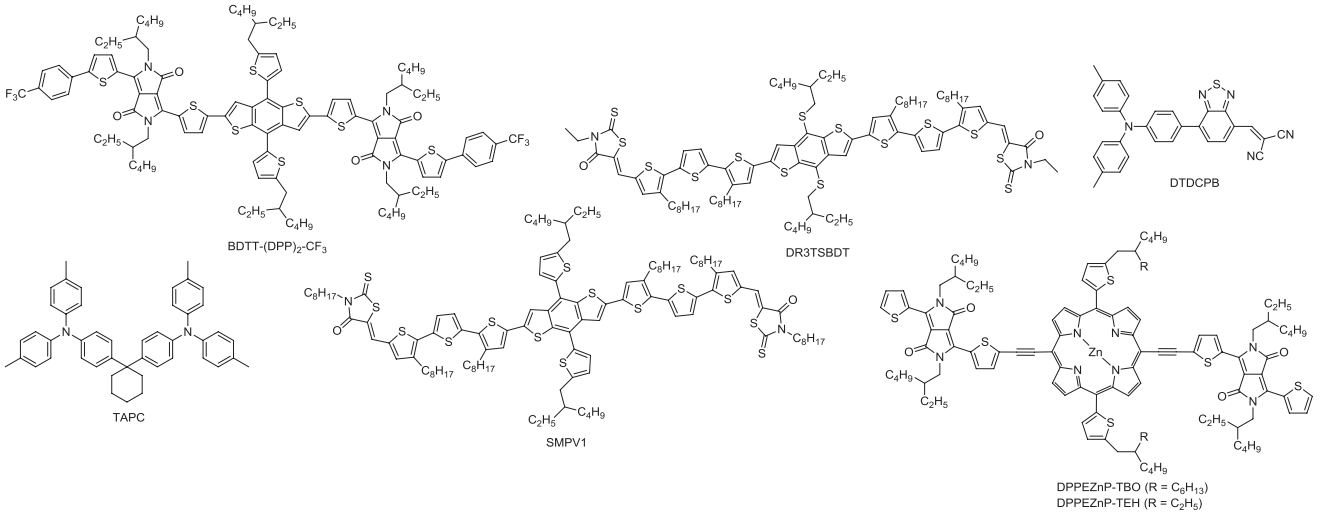

Figure 7. Small-molecular donor materials used in tandem solar cells. The references for publications describing these materials are provided in Table 1.

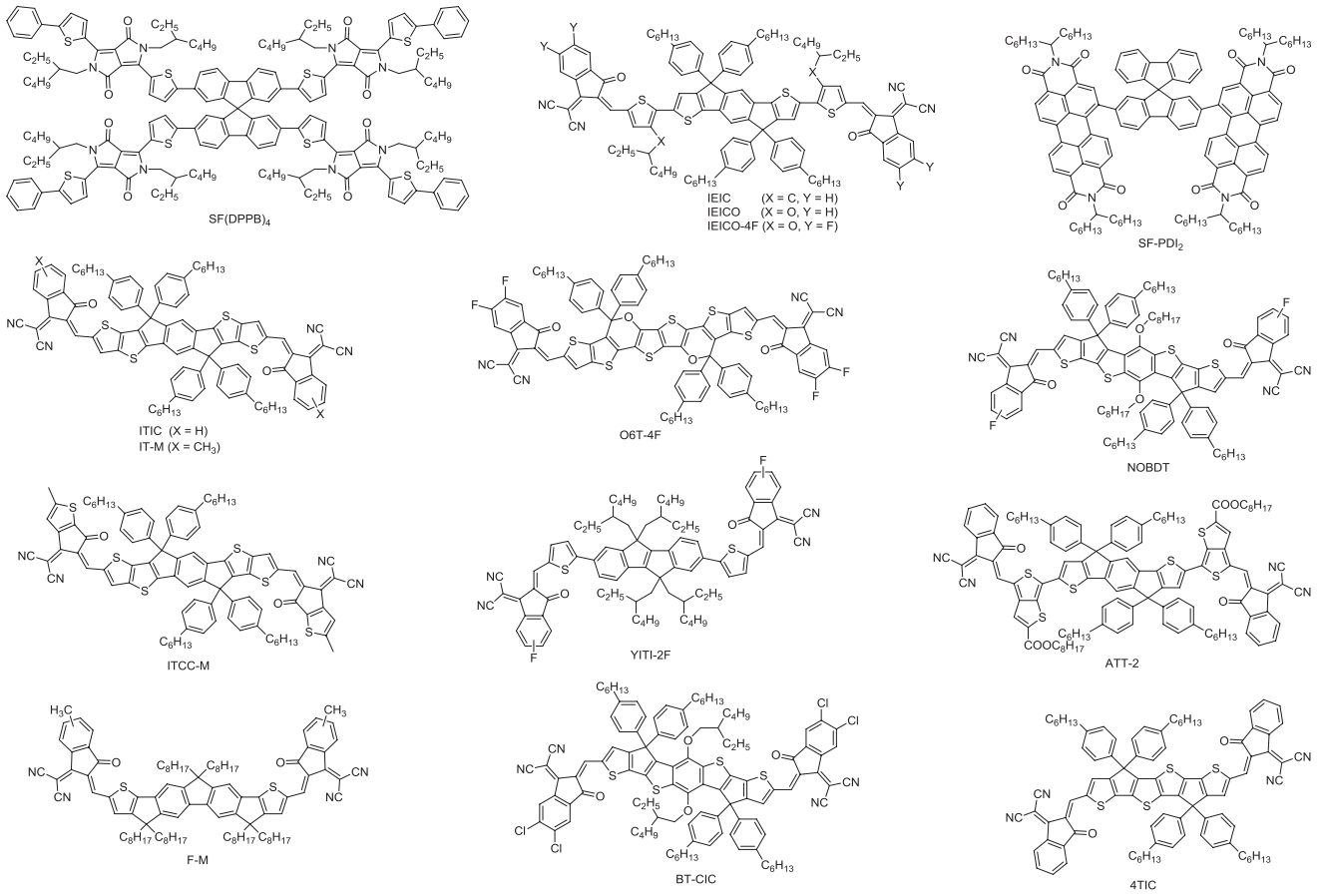

Figure 8. Nonfullerene acceptor materials used in tandem solar cells. The references for publications using these materials are provided in Table 1.

and PDPP4T, respectively. A tandem with PBDD4T-2F:$PC_{60}BM$ (V_{OC} = 0.90 V) as front cell and PDPP4T-2F:$PC_{70}BM$ as back cell afforded a high V_{OC} of 1.68 V, together with a J_{SC} of 11.3 mA cm^{-2} and a PCE of 11.6%. Benefitting from the successful development of benzodithiophene (BDT)-based polymers, Duan et al. reported a thienyl-substituted BDT copolymerized with fluorine-substituted benzothiadiazole (BT) and two thiophenes (BDT–FBT–2T).[86] The optical bandgap of this polymer amounted to 1.72 eV. Single-junction solar cells with a blend of this polymer with $PC_{70}BM$ showed no loss of performance at increasing thickness of the active layer up to 250 nm. Both characteristics make it suitable as front cell wide bandgap donor material in a tandem device. Using PMDPP3T:$PC_{60}BM$ as back cell, a tandem with a PCE of 8.9% was fabricated, for which the main limiting factor was the V_{OC} (1.42 V), due to the significant minimum photon energy loss (E_{loss} = 0.85 eV) in the front cell. Furthering on the BDT unit as leitmotif, PTZ1 was synthesized in 2016 by Guo et al. by copolymerization with the

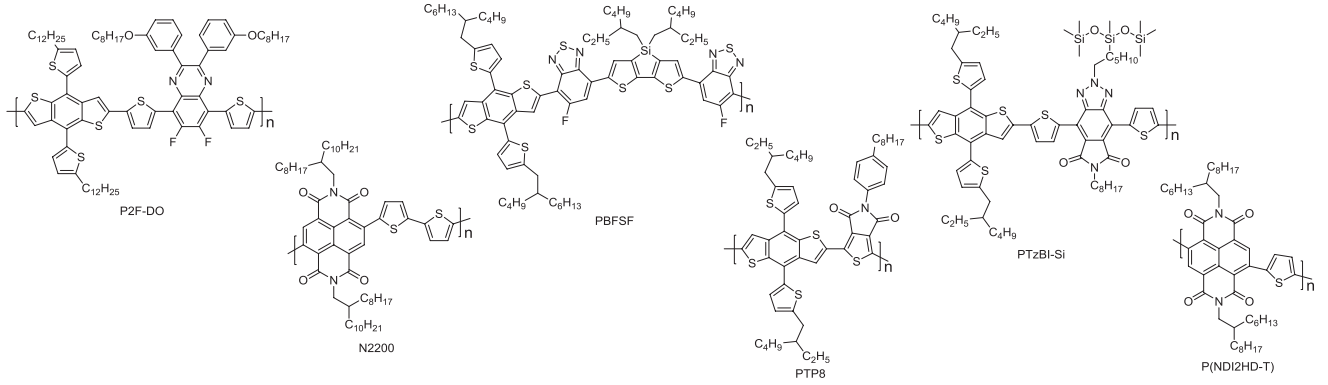

Figure 9. Donor and acceptor materials for all-polymers blends reported in tandem solar cells. The references for publications using these materials are provided in Table 1.

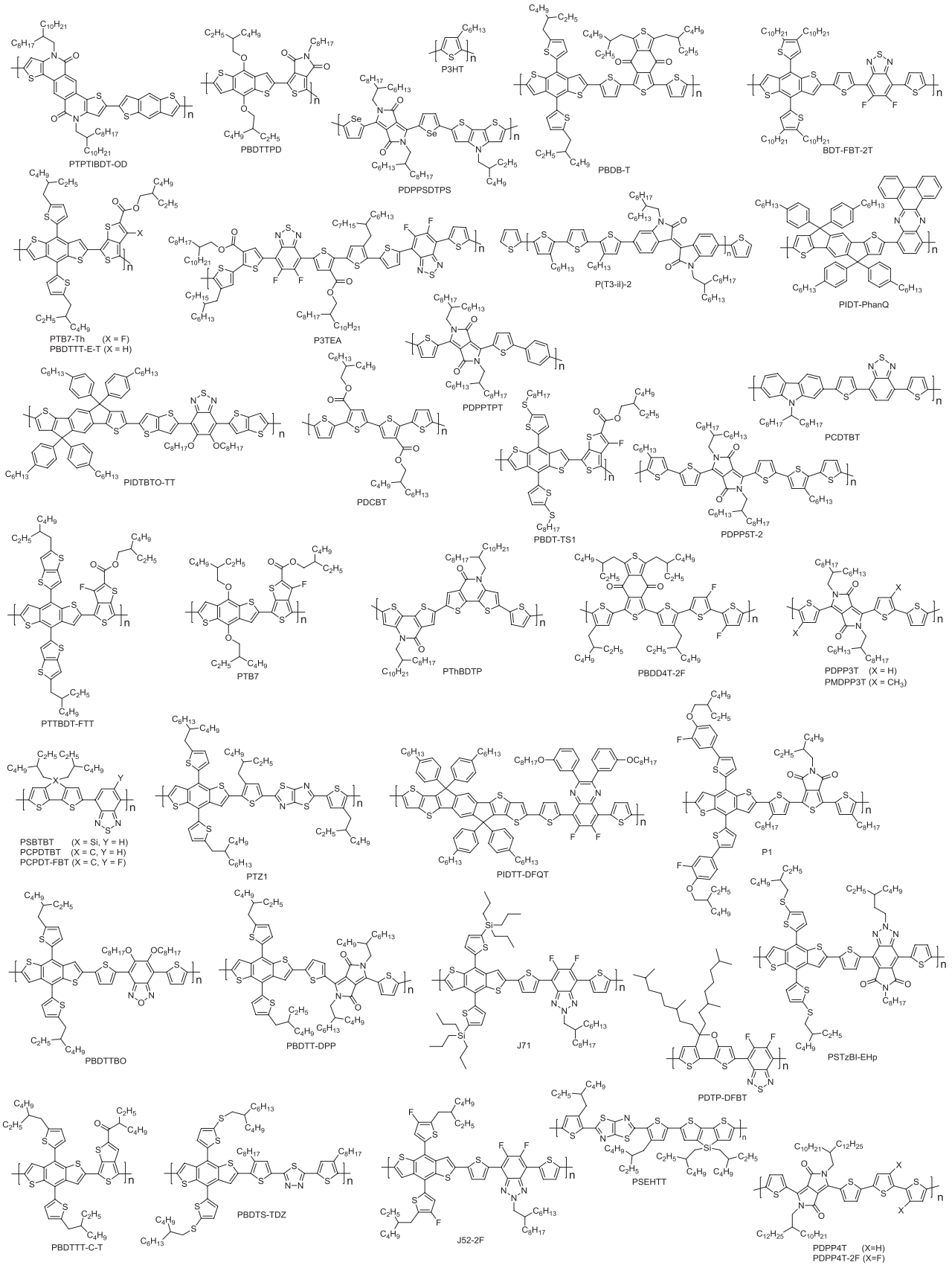

Figure 10. Polymer donor materials used in tandem solar cells. The references for publications describing these materials are provided in Tables 1 and 2.

electron deficient thiazolothiazole unit.[87] Because of the wide bandgap of 1.97 eV and the relatively deep-lying HOMO level of −5.31 eV, a high V_{OC} of 1.01 V was measured for the pristine PTZ1:$PC_{70}BM$ single-junction solar cell, which lowered to 0.94 V after optimization of the processing conditions. These materials were adopted in a tandem as front cell, with a blend of the low bandgap (1.58 eV) PBDTTT-C-T and $PC_{70}BM$ in the back cell. The latter was reported to give a V_{OC} of 0.74 V. The tandem gave a PCE of 10.3%, with a nearly ideal addition of the V_{OC} (1.65 V), FF of 0.65, and J_{SC} of 9.6 mA cm^{-2}. Integration of the EQE of the subcells gave 8.15 and 9.80 mA cm^{-2} for the front and back subcells, respectively. Indacenodithiophene (IDT) is an interesting donor unit for donor–acceptor (D–A) copolymers given the planarity of its structure. A new copolymer of IDT with BT units was reported by Ma et al. (PIDTBTO-TT).[82] The authors copolymerized these units using thienothiophene (TT) as π-bridges. After optimization of the morphology using $PC_{70}BM$ as acceptor and diiodooctane as cosolvent, a PCE of 8.15% was found. Since the polymer had a bandgap of 1.87 eV and gave a V_{OC} of 0.91 V, it was used as front cell of a tandem, in combination with PTB7-Th:$PC_{70}BM$ in the back cell. A V_{OC} of 1.70 V and a PCE of 11.2% were achieved for the best device. More BDT-based donor polymers, P1 and P2, were reported by Song et al.[88] For an optical bandgap of 1.82 eV, 0.91 and 1.00 V of V_{OC} were achieved in single-junction devices with $PC_{70}BM$, thanks to deep-lying HOMO levels of −5.43 and −5.50 eV, respectively. The single junctions were also characterized by EQE spectra of 70%. These materials were used as front cell for two different tandem solar cells, in combination with PTB7-Th:$PC_{70}BM$ (V_{OC} = 0.81 V) in the back cell. From the measurements, V_{OC} values of 1.64 V (with P1) and 1.72 V (with P2) were obtained. The measured J_{SC}s were 10.1 mA cm^{-2} (P1) and 9.3 mA cm^{-2} (P2) and lower J_{SC}s were integrated from the EQE spectra of the subcells.

In recent years increasing focus in the OPV field is on nonfullerene acceptors (NFAs).[89–92] NFA molecules allow more freedom to engineer the energy levels (and optical bandgap) to achieve high V_{OC}. Different from fullerene-based acceptors, a reduced offset in the HOMO–HOMO and LUMO–LUMO of donor and acceptor does not occur at the expense of efficient charge separation.[93] Studies suggested a different nature of the exciton separation process in this class of systems. In addition, the photocurrent can benefit from their substantial absorption coefficient. Although the anisotropy limits the number of successful donor–acceptor combinations, an increasing number of relevant results have been reported in the last few years, with important consequences on the efficiency not only of single-junction but also of tandem solar cells. The review paper by Cheng et al. provides a good overview of recent results about nonfullerene polymer solar cells and the direction to further advance in this field. Hou et al. also analyzed the opportunities and challenges of NFAs. For a more in-depth discussion of the topic, the reader is referred to recent review papers.[89–92] A first demonstration of how a high V_{OC} can be achieved in tandems with NFAs was given by Liu et al. in 2016.[94] Two polymer:NFA systems with high V_{OC} and complementary absorption were selected for their tandem: P3HT:$SF(DPPB)_4$ (the bandgaps are 1.90 and 1.77 eV, respectively) and PTB7-Th:IEIC (bandgaps of 1.58 and 1.50 eV, respectively). The first one delivered a V_{OC} of 1.11 V, while the second one gave 0.95 V. The best tandem device (PCE = 8.48%) afforded a V_{OC} as high as 1.97 V. The performance in this case was mainly limited by the FF (0.52), largely determined by the FF of the corresponding single-junction cells (0.54 and 0.47 for the front and back subcells). The highest V_{OC} for an NFA tandem was reported by Chen et al.[65] With P3TA (bandgap = 1.72 eV) and $SF\text{-}PDI_2$ (bandgap = 2.07 eV) as polymer donor and NFA, respectively, a low voltage loss could be achieved (0.6 eV). Due to the limited absorption in the optimal single-junction device, combining the same active layer blend as both front and back subcells in a homo tandem allowed to boost the efficiency from 9.5% (single junction) to 10.8% (tandem), accompanied by a remarkable V_{OC} of 2.13 V. In 2017 multiple NFA systems introduced in tandem solar cells allowed to break the 12% efficiency threshold, surpassing the current state-of-the-art for fullerene-based tandems. Shi et al. reported an efficient low bandgap NFA by combining a central fused rings electron-donating unit, thiophene–thienothiophene–thiophene (4T), with a terminal electron-accepting part, 3-(dicyanomethylidene)indan-1-one (IC), resulting in 4TIC.[95] Given the shallower HOMO level and slightly deeper LUMO level than the benchmark NFA named ITIC (bandgap of 1.59 eV), the 4TIC is characterized by an energy gap of 1.40 eV. Blended with PTB7-Th as donor, 4TIC demonstrated 10% efficiency in a single-junction cell, owing to a J_{SC} of 18.4 mA cm^{-2}, together with a V_{OC} of 0.78 V and an FF of 0.72, which makes it suitable as back cell for tandems. Therefore, the authors combined it with PBDB-T:ITIC (PBDB-T has a bandgap of 1.80 eV) as front cell, which is capable of 0.92 V of V_{OC}, and J_{SC} and FF of 16.1 mA cm^{-2} and 0.71, respectively. The tandem afforded a V_{OC} of 1.65 V, a high FF of 0.71, and a J_{SC} of 10.6 mA cm^{-2} (PCE = 12.6%). No EQE spectrum was reported. Qin et al. profited of the even lower bandgap of the IEICO acceptor (1.34 eV), which together with PBDTTT-E-T (1.55 eV) as donor showed PCE over 9% in single-junction configuration, with a V_{OC} of 0.81 V.[96] In a tandem with this blend as back cell and PBDD4T-2F:$PC_{70}BM$ as wide bandgap front cell (V_{OC} = 0.90 V), a PCE of 12.8% could be obtained at best, with a V_{OC} of 1.71 V and a J_{SC} of 11.51 mA cm^{-2}. The EQE of both subcells in particular was over 60%, and extended to ≈900 nm. To achieve a wider bandgap than ITIC, Cui et al. synthesized its derivative ITCC-M, for which the bandgap was 1.68 eV.[36] Single-junction cells of PBDB-T:ITCC-M were characterized by a V_{OC} of 1.03 V, in addition to a J_{SC} of 14.5 mA cm^{-2}, reflecting the EQE up to ≈75%. Again using PBDTTT-E-T:IEICO as back cell and the blend of the new NFA in the front cell, the authors could push the PCE to 13%, where the V_{OC} was 1.79 V and the J_{SC} was 11.4 mA cm^{-2}. In 2018, the same group improved the efficiency with respect to the latter result by carefully choosing more suitable materials for the active layers.[97] Instead of PBDB-T:ITCC-M, they adopted the wide bandgap (1.94 eV) polymer J52-2F (also known as PFBZ) in the front cell, blended with IT-M, for which the bandgap is 1.60 eV. Due to the wider and lower bandgap of J52-F and IT-M, respectively, the EQE featured higher values in the range where the polymer absorbs and it was extended up to almost 800 nm thanks to the acceptor. At the same time, the minimum photon energy loss was also decreased from 0.69 to 0.64 eV and the FF remarkably increased to 0.73. For the back cell, the spectral

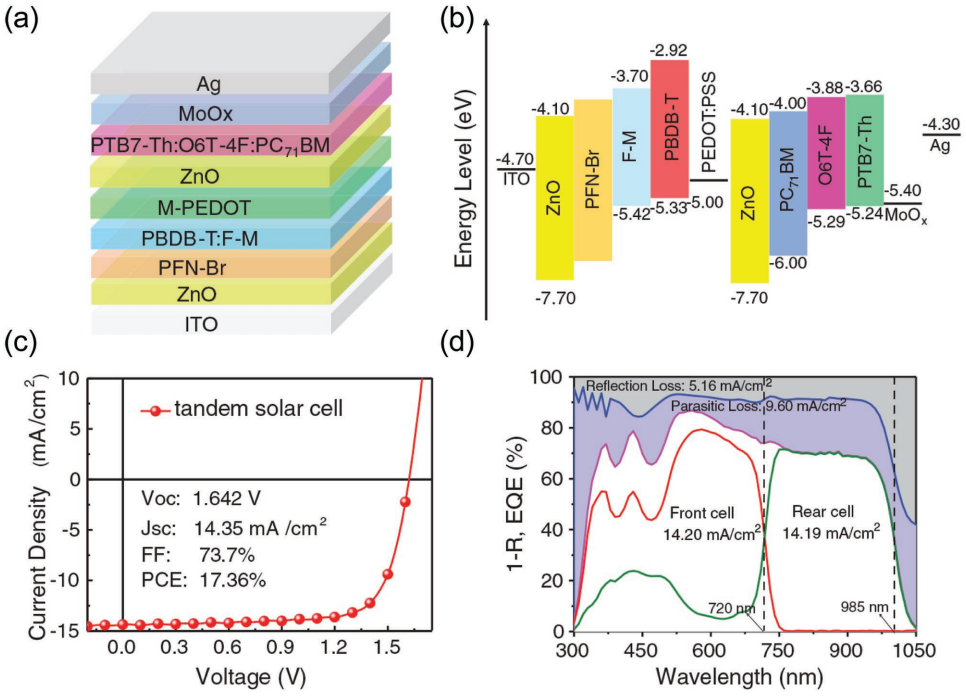

Figure 11. Record efficiency (17.4%) tandem organic solar cell. a) Device stack. b) Energy level diagram. c) *J–V* characteristic and device metrics. d) EQE of the subcells measured under relevant light and voltage bias conditions. Reproduced with permission.[102] Copyright 2018, The American Association for the Advancement of Science.

response was upshifted to 1000 nm by using the NFA IEICO-4F, which has a lower bandgap of 1.24 eV (instead of 1.34 eV of IEICO). This one was blended with the donor PTB7-Th and together in a single-junction device, they gained a higher EQE over the whole spectral range, without drop in FF (0.69). The combination of these two active layers yielded a tandem with best efficiency close to 15% (14.0% certified), thanks to a slightly lower minimum photon energy loss, significantly higher current (J_{SC} = 13.3 mA cm^{-2}) deriving from the broader absorption, and improved FF of 0.68 (V_{OC} = 1.65 V). Another reported tandem featuring PTB7-Th:IEICO-4F as low bandgap back cell was demonstrated by Shi et al.[98] A high PCE of 14.1% was also reported by Zhang et al. for an NFA-based tandem.[99] Two new NFAs were synthesized ad hoc, F-M (bandgap 1.65 eV) and NOBDT (bandgap 1.39 eV) and blended with PBDB-T (1.80 eV) and PTB7-Th (1.58 eV), respectively. Both these blends in single-junction cells showed generally very good photovoltaic performance. It is noted that both returned EQE values ≥70%. The F-M blend and the NOBDT blend were used as front and back subcells in a tandem cell, respectively. This device yielded high V_{OC} (1.71), high FF (0.70), and J_{SC} of 11.72 mA cm^{-2} at the same time. Yue et al. reported a newly developed NFA with medium bandgap (1.64 eV) based on the indenoindene core, named YITI-2F.[100] This NFA was blended with PBDB-T, reaching an efficiency of 9.7% in single junction, with a V_{OC} of 0.93 V, a J_{SC} of 15.5 mA cm^{-2}, and an FF of 0.70. They adopted this system as front cell of a tandem. For the back cell, PTB7-Th:ATT-2 was selected, ATT-2 being a previously reported NFA with bandgap of 1.32 eV. In a single junction, the latter gave PCE of 9.52%. The tandem reached an efficiency of 11.9% at best, mainly limited by the intensity of the EQE, with maxima of ≈50% and 60% for the front and back subcells, respectively, and the spectral coverage up to ≈950 nm. As alternative to the synthesis of a new NFA matched to the donor polymer, the opposite strategy is also a valid option. Xu et al. selected the ITIC acceptor and blended it with a newly developed donor polymer: PBDTS-TDZ, which has a bandgap of 2.09 eV.[101] The blend used for the active layer afforded a remarkable PCE of 12.8% already in single-junction configuration. Subsequently, a homo-tandem device was fabricated, which yielded a high current density, and in turns an outstanding PCE of 13.4%.

The highest efficiency reported for an organic solar cell is for an all solution–processed tandem cell featuring polymer:NFA blends in both front and back cells. In 2018, Meng et al. reported a combination of photoactive materials leading to a significantly higher PCE of 17.4%.[102] With respect to the previous work from reference,[99] the single-junction devices of the front and back cells afford a substantially higher J_{SC}, at the expense of only a modest drop in V_{OC}. One of the main reasons for this simultaneous improvement could derive from the use of the inverted architecture, in which the silver top contact has better reflectivity than aluminum (**Figure 11**). In the inverted configuration, the same PBDB-T:F-M single-junction cell featured a higher EQE of 0.80. For the back cell, a ternary blend of PTB7-Th:O6T-4F:$PC_{70}BM$ was adopted, where O6T-4F is an NFA (also known as CO_i8DFIC) with bandgap of 1.26 eV. With respect to the binary PTB7-Th:O6T-4F system, the ternary blend has a redshifted absorption up to about 1050 nm, possibly induced by a morphological change due to the presence of PCBM. Consequently, the single junction gave J_{SC} of 28 mA cm^{-2}. In the tandem, these high and broad EQEs of the corresponding single junctions permitted to redistribute the

amount of light of the solar spectrum between the subcells, leading to a balanced J_{SC} of 14.2 mA cm^{-2} from both. This record value of J_{SC} for OPV tandems largely overcompensated the 60 mV loss of V_{OC} with respect to reference,[99] holding at the same time an FF of 0.74.

Few examples of small-molecular donor materials blended with PCBM in combination with a tandem cell configuration have been reported since 2015. Kim et al. optimized the performance of a benzodithiophene-diketopyrrolopyrrole-based small molecule by introducing trifluoromethylbenzene end groups, resulting in BDTT-(DPP)$_2$-CF$_3$.[103] This molecule has a bandgap of 1.55 eV and returned a PCE of 6% at best in single junction, blended with PC$_{70}$BM (V_{OC} = 0.70 V). This active layer was incorporated as back cell in a tandem solar cell, where P3HT:ICBA was used in the front cell. The tandem showed a V_{OC} of 1.53 V, with an FF of 0.68 and a J_{SC} of 8.0 mA cm^{-2}, resulting in a PCE of 8.11%. The main limit to the efficiency of the tandem was the low EQE of the back cell (max. 60%). Zhang et al. reported the application of a high performing, wide bandgap, small molecular donor material, named DR3TSBDT in tandem cells.[81] This molecule has a bandgap of 1.74 eV and when blended with PC$_{70}$BM it showed very interesting properties in single-junction cells: V_{OC} = 0.91 V, J_{SC} = 14.3 mA cm^{-2}, and FF = 0.71 (best PCE of 9.5%). This makes it interesting as front cell for tandem solar cells. As back cell, the authors chose PTB7-Th:PC$_{70}$BM (V_{OC} of 0.80 V). The tandem yielded a best PCE of 11.5%, corresponding to an FF of 0.65, a V_{OC} of 1.69 V, and a J_{SC} of 10.51 mA cm^{-2}. The spectral overlap with the PTB7-Th cell leaves room for improvement, provided a lower bandgap back cell is adopted instead. The same DR3TSBDT:PC$_{70}$BM active layer was integrated in a tandem with another small molecular donor:PC$_{60}$BM blend by Li et al.[104] The latter was a zinc porphyrin–based molecule, DPPEZnP-TBO, with a low bandgap of 1.37 eV. Thanks to a low minimum photon energy loss, DPPEZnP-TBO:PC$_{60}$BM had a V_{OC} of 0.73 V in single-junction cells, and EQE up to ≈900 nm (maximum of ≈60%). By combining the latter in a tandem as back cell, with DR3TSBDT:PC$_{70}$BM as front cell, a best efficiency of 12.5% was demonstrated, the highest for solution-processed small-molecular donor systems.

It is certainly worth to discuss the first example of an all-polymer (i.e., polymer donor and polymer acceptor) tandem solar cell, reported in 2016 by Yuan et al.[105] P2F-DO and N2200 were blended as donor and acceptor polymers, respectively. The first one has a bandgap of 1.60 eV while the second one has a bandgap of 1.45 eV. The optimal single-junction cell absorbed up to ≈800 nm and had a V_{OC} of 0.80 V. The PCE was limited to 4.7% because of the low EQE (≈40%). To improve the light absorption, a homo tandem with this materials was manufactured. This one showed the same FF (0.58) and almost twice the V_{OC} (1.58 V) of the single-junction device. Recently, Yuan et al. reported an improved all-polymer tandem, using complementary absorber layers.[106] For the front cell, a combination of polymers with similar wide bandgap was used: the BDT-based PTP8 (bandgap of 1.80 eV) as electron-donating species, and P(NDI2HD-T) (bandgap of 1.85 eV) as electron-accepting component. For the back cell, a newly synthesized ternary conjugated polymer, PBFSF (bandgap of 1.55 eV) was used as donor, while N2200 was the acceptor. The J_{SC} of the tandem was almost 8 mA cm^{-2} and the V_{OC} was 1.77 V, together with an FF of 0.59. The PCE was then 8.3%. A new record PCE for all-polymer tandem cells was established in 2018 by Zhang et al.[40] Again a homo tandem was fabricated, adopting PTzBI-Si as donor and N2200 as acceptor. The first one has a bandgap of 1.78 eV, and when blended with N2200 it returned a V_{OC} of 0.86 V in a single-junction configuration, together with a remarkable FF above 0.7, and a J_{SC} of 15.4 mA cm^{-2}. The tandem cell was characterized by an improved overall absorption, according to the J_{SC} (8.6 mA cm^{-2}) of the current-limiting subcell, while V_{OC} and FF were in agreement with the expectation from the single-junction cell, affording a PCE of 11%.

2.5. Upscaling

For the future commercial application of solution-processed tandem organic solar cells, it is important to further develop manufacturing technology and device configurations that enable large area and roll-to-roll production. Many high-efficiency tandem solar cells require processing of layers in an inert atmosphere environment. This constraint limits large-scale production. Solution-processed tandem OPV cells have therefore also been studied in relation to technology related aspects such as processing under ambient atmosphere, increase in device area by interconnecting tandem cells into a module, and processing electrodes from solution.

Li and Brabec reported air-processed tandem solar cells with efficiency exceeding 10%.[107] Not only the ZnO, PEDOT:PSS and PEI charge transport and interconnecting layers were deposited in ambient air by blade coating, but also the photoactive layers. For the front cell a commercial polymer (GEN-2) blended with PC$_{60}$BM was adopted, while for the back cell, the well-known PTB7-Th:PC$_{70}$BM was used. In their work, the authors pointed out the critical drop in performance of the back cell due to the manufacturing in ambient air. A solvent treatment with ethanol was observed to recover the performance, which they speculate could remove residual diiodooctane, used as cosolvent for the active layer. To process the active layer blends under safe conditions, it is important to address the problem of the toxicity of the solvents used. Typically to achieve optimal performance, these materials are processed from (mixtures of) halogenated solvents. Xu et al. demonstrated highly efficient homo-tandem solar cells where the active layers were processed exclusively from *o*-xylene, which is relatively safe.[101] The combination of photoactive materials used in each subcell consisted of PBDTS-TDZ as donor and ITIC as acceptor. Interconnection of the subcells was realized by means of a sequence of PEDOT:PSS/ultrathin Ag/ZnO nanoparticles. The processing of the active layer from *o*-xylene afforded a remarkable PCE of 13.4%.

Another important factor to scale the technology is achieving high efficiencies for larger area devices. Tandem modules of 1.3 and 2.1 cm^2 with PCEs of 5.2% and 4.7% were reported by Hanisch et al.[108] In the two cases, 3 and 5 cells were connected in series, respectively. Also in this work, all layers except the electrodes were deposited in ambient air by doctor blade coating, a technique in which the drying is similar to slot-die coating. For the active layers, they used PCDTBT and

Si-PCPDTBT (also known as PSBTBT) for the front and back subcells, respectively, and $PC_{70}BM$ as acceptor. For the ICL, ZnO nanoparticles and pH–neutral PEDOT:PSS/Nafion were adopted. A combination of laser and mechanical scribing was used for the patterning at the lines interconnecting the cells. Although the series resistance of the electrodes increases with the size of the cell, the shunt resistance can benefit from the increased number of layers in a tandem, with respect to a single-junction structure, as demonstrated by Mao et al.[109] In their work, they created single-junction and tandem solar cells with a size of 0.73 and 1 cm^2, respectively. They intentionally created ≈1 mm^2 size defects either in the front cell or the interconnecting layer. Consequently, they detected only a modest drop in performance for the tandem, while the single-junction cell underwent a more dramatic loss in performance. On a flexible polyethersulfone (PES) substrate, they built a 10.5 cm^2 size tandem cell, which afforded an efficiency of 6.5%, fairly close to the PCE of 7.7% of the small size reference tandem (0.05 cm^2). The PES substrate was coated with evaporated silver, followed by a thin layer of PEI. P3HT:ICBA and PTB7-Th:$PC_{60}BM$ were used as active layers for the front and back subcells and modified PEDOT:PSS/PEI formed the ICL. PEDOT:PSS (modified PH1000) was also used as top electrode, followed by evaporation of silver grid lines with 5% shadowing loss. All the nonmetallic layers were deposited by spin-coating. The optimization of the front and back cell layer thickness can be done either via opto(electrical) modeling or experimentally, by realizing multiple tandem cells with different thickness of the active layers. In 2018 Glaser et al. proposed a simple method to optimize the time consuming experimental screening of the optimal thicknesses of the subcells.[110] To do so, they manufactured tandem solar cells on a single 4 × 4 cm^2 substrate by blade coating technique. PTB7:$PC_{70}BM$ was used as active layer for both the front and back subcells. For the front cell, they created a wedge-shape thickness profile in one direction. The substrate was then rotated by 90° and the back cell deposited with a similar thickness wedge. In this way a grid of different thickness combinations for the front and back subcells was determined. The substrate was illuminated through a small aperture, which was moved along a grid of positions to map the photocurrent. Upscaling one specific combination of thicknesses to a 4-cell module of 24 cm^2 afforded a PCE of 5.2%, with geometric fill factor of 84%.

Indium-doped tin oxide is undoubtedly the most used and best performing transparent electrode for organic solar cells. Unfortunately, the coating of this material requires low-throughput vacuum-based techniques, such as sputtering. In addition, its application on flexible substrates is limited by its brittleness. On top of this, the availability and in turn the price of indium significantly raise the production costs. In this sense, some studies explored the use of silver instead of ITO, deposited as a semitransparent grid or as a nanowire layer.[109,111,112] Guo et al. demonstrated a fully solution-processed tandem polymer solar cell using silver nanowires from a commercially available dispersion for the semitransparent contact.[112] Interestingly, also the opaque contact was deposited from a commercially available silver ink, which was cured at relatively low temperature (130 °C), compatible with flexible substrates. It is worth to mention this since the reference opaque contact in almost every work on OPV consists of a metal deposited by thermal evaporation in high vacuum. By depositing all the layers by doctor-blade coating in ambient conditions, the authors presented a 5.81% tandem on glass and a 4.85% tandem on flexible polyethylene terephthalate substrates. The commercially available GEN-2 and PDPP5T-2 blended with PCBM were used a front and back subcells, respectively. The ICL was made of zinc oxide nanoparticles and pH–neutral PEDOT:PSS. Also gold-doped single-layer graphene nanoribbons (SLGNR) were employed as replacement of ITO by bin Mohd Yusoff et al.[113] The procedure adopted in this work to create such an electrode started from the growth of graphene from chemical vapor deposition on copper substrate. Thorough a series of steps, single-layer graphene nanoribbons were isolated and dispersed in water with gold chloride, after which additional steps followed, leading to the end product. The tandem device was built on a glass substrate covered with the Au-doped SLGNR, followed by PEDOT:PSS and thermally evaporated tungsten oxide (4 nm). SMPV1:$PC_{70}BM$ and PTTBDT-FTT:$PC_{70}BM$ were adopted for the front and the back subcells, respectively. For the ICL, a nonspecified combination of materials was involved: solution-processed zinc oxide was cast on the front cell, on top of which PEDOT:PSS (probably at neutral pH) was stacked. The device was completed with evaporated Ca/Al. The measurement of the *J–V* characteristic provided a V_{OC} of 1.56 V (1.62 V expected) and an FF of 0.64 (close to the corresponding single-junction cells). The authors reported EQE spectra for the subcells which added to each other closely approach 100% at some wavelengths. Another interesting semitransparent electrode from solution is the highly conductive formulation of PEDOT:PSS. Tong et al. provided an example where they used such a highly conductive PEDOT:PSS (PH1000) as a transparent top electrode for tandem solar cells, deposited by film transfer.[114] Their tandem device consisted of P3HT:ICBA as both front and back subcells and PH1000/PEI as ICL. For the top electrode, first a piece of polydimethylsiloxane (PDMS) was attached on a glass substrate. Before depositing a modified PH1000 dispersion, the PDMS surface was treated with oxygen plasma to improve the wetting. Once formed, the layer of PEDOT:PSS was dried at room temperature. Then the surface of top cell was also treated with oxygen plasma for 5 s. The PDMS/PEDOT:PSS was applied on this active layer, with the PEDOT:PSS in contact with it, and the PDMS stamp was peeled off. In 2016, the same group reported the use of transfer printed PEDOT:PSS top electrode on a fully solution-processed tandem solar cell on flexible PES substrate.[115] A modified PH1000 dispersion was used as bottom electrode, patterned by selective surface treatment of the substrate with oxygen plasma. To build an inverted tandem, the PH1000 surface was modified with PEI, for the bottom electrode. P3HT:ICBA and PTB7-Th:$PC_{70}BM$ were used as front and back cell active layers, and a modified PEDOT:PSS (mixture of Al4083 and PH1000) followed by PEI was used as ICL. The PCE reached by the device was 6.1%, limited mainly in current because of the absence of a reflecting electrode.

With increased efficiencies the stability of tandem solar cells becomes an important topic for the future. Krebs, Brabec, and coworkers addressed this issue in two publications.[116,117] One issue is that ETL materials like AZO (on the ITO contact) and ZnO (in the ICL) require a treatment with UV light to increase

their conductivity and attain optimal performance. To address the stability of this UV photodoping, the *J*–*V* characteristics of such tandem cells were characterized under simulated AM1.5G solar radiation (100 mW cm^{-2}), after different periods of photoaging under white light illumination without UV component.[116] The cells were manufactured on glass substrates under ambient conditions by blade coating, and encapsulated with a glass protection. In a first test the persistence of the light-soaked state was assessed. Already after 50 h, the PCE lowered to ≈60% of the initial value, due to a concomitant decrease in J_{SC} and FF. Another test followed, in which before each measurement, the device was illuminated under a UV light source (365 nm) for 10 s to reactivate the metal oxides. In this case a loss in FF was the main responsible for the drop in PCE with time (11% loss after 2000 h) with respect to its initial value. To see this result in perspective, the authors performed the same test on the corresponding single-junction cells of the subcells in the tandem. The outcome was that the single-junction devices lost 15%–16% of their initial efficiency after the same 2000 h period.[116] The stability of tandem cells was further assessed in an interlaboratory study, following the recommendations from different protocols from the International Summit on OPV Stability (ISOS), both in the dark and under illumination.[117] In these tests, both tandem and the corresponding single-junction solar cells were fabricated on flexible, ITO-free substrates by roll coating and encapsulated either between two glass slides with a UV-curable adhesive or using a commercial barrier foil. Following the three protocols, all types of cells behaved similarly. For the one under light soaking an initial fast decay in maximum power down to less than 60% of the initial value was also observed, within the first 50 h.

These studies provide encouraging evidence for a comparable stability of tandem and single-junction OPV cell configurations. Of course the stability of OPV devices remains an issue for future development of this technology. The stability of OPV devices is affected by factors such as metastable morphology, ingress of water and oxygen, diffusion of electrodes or interlayers, photochemical stability, mechanical stress, and heating. We refer to recent reviews on this topic for further information.[118–120] For protecting the device from humidity, OPV technology could profit from findings emerged in the field of perovskite solar cells. Bella et al. demonstrated the effectiveness of photocurable fluoropolymers as encapsulation on both the transparent as well as the opaque side of the device.[121] Alternative, Lv et al. reported that a trilayer of Al_2O_3/O–Al–$(CH_3)_{3-x}$/Al_2O_3 deposited by atomic layer deposition (ALD) on top of the metal contact of a perovskite solar cell, provides good stability against moisture.[122] Next to the compact ALD Al_2O_3 layers, the intermediate reactant in between the two Al_2O_3 films acts as a scavenger of the few water molecules permeating the external layer. Interestingly, the deposition temperature inside the ALD machine chamber was only 60 °C. In our view, both approaches developed in refs. [121] and [122] are in principle compatible with OPV technology, and they may therefore stimulate researchers to direct their effort toward those directions.

Related to future technology development, few more studies focused on the process control of the manufacturing by imaging/probing techniques.[123–125]

3. Triple- and Quadruple-Junction Solar Cells

In principle, increasing the number of junctions in a multijunction solar cell allows to progressively increase the efficiency.[126] In practice this idea is very difficult to pursue, especially when the manufacturing is performed via solutions. Developing highly performing active materials with complementary absorption also poses challenges to the practical realization. In the period 2015–2018, only few triple-junction solar cells from solution processing have been reported.

The highest efficiency published until the end of 2014 for all solution–processed triple-junction solar cells was 11.6% by Chen et al.[26] In 2015 bin Mohd Yusoff et al. developed another triple cell, aiming at achieving a higher efficiency.[127] In their report, PSEHTT (bandgap of 1.82 eV) blended with ICBA was used as wide bandgap front cell, while PTB7 (bandgap of 1.61 eV) and PMDPP3T (bandgap of 1.30 eV) were adopted as middle and low bandgap polymers for the middle and back subcells, respectively, both blended with $PC_{70}BM$. The device structure was inverted, and the interconnection of the subcells was realized by a stack of pH–neutral PEDOT:PSS, followed by lithium-doped zinc oxide (LZO) from a sol–gel route and a self-assembled monolayer of C_{60}, also from solution. The triple cell provided V_{OC} = 2.24 V, J_{SC} = 7.83 mA cm^{-2}, and an FF of 0.68, pointing toward a PCE of 11.8%. Regrettably, the characterization of this triple cell is not completely consistent, because the summed EQE of the subcells exceeds 100%. In 2016, Gao et al. reported both double- and triple-junction solar cells using PBDTTPD:$PC_{70}BM$ as absorber material for all the subcells.[128] The aim was to use these cells for photoelectrochemical water splitting. The homo tandem and triple cells can potentially not only afford the high photovoltage required, but they can also increase the efficiency by increasing the light absorption, which was limited in their optimal single junction. They fabricated the multijunction cells with a conventional structure, with a solution-processed zinc oxide nanoparticles layer, followed by thermally evaporated Al and MoO_3 as ICL. The bottom contact was ITO/PEDOT:PSS and the top contact was Ca/Al. The triple featured a V_{OC} of 2.75 V, in perfect agreement with the V_{OC} of 0.92 V (at best) of the single junction, and an FF of 0.68. With respect to the tandem cell, the efficiency of the triple-junction cells was lower (PCE of 8.35% for the tandem and PCE of 7.42% for the triple), likely due to the fact that the tandem already afforded a nearly complete absorption of light. Two additional examples about the use of triple-junction polymer solar cells for water splitting will be discussed in Section 5.[129,130] Di Carlo Rasi et al. reported three triple-junction solar cells fabricated using the same PEDOT:PSS/zinc oxide ICL, also discussed in Section 2.2.[67] Briefly, the commercial PEDOT:PSS dispersion was diluted with 1-propanol and deposited in inert atmosphere on one active layer, a film of ZnO nanoparticles was stacked on top by processing from isoamyl alcohol. These devices were made with an inverted device structure, using sol–gel zinc oxide on the ITO bottom contact and evaporated molybdenum oxide/silver as top contact. A first device used PCDTBT:$PC_{70}BM$, PDPPTPT:$PC_{60}BM$ and PDPP5T:$PC_{60}BM$ for the front, middle and back subcells, respectively. These absorbers have different and complementary bandgap of, in order, 1.88, 1.53 eV and 1.46 eV. The triple junction featured

a V_{OC} of 2.26 V, perfectly matched to the sum of the single-junction cells: 0.88, 0.79, and 0.57 V, in the stack. A second device with PDCBT:$PC_{60}BM$ (front cell), PDPPTPT:$PC_{70}BM$ (middle cell) and PMDPP3T:$PC_{60}BM$ (back cell) was fabricated. PDCBT and PMDPP3T are better performing materials with bandgaps of 1.90 and 1.30 eV, respectively. The bandgap of 1.30 eV of PMDPP3T created a redshifted absorption compared to PDPP5T. The use of $PC_{60}BM$ in the front and back subcells and of $PC_{70}BM$ in the middle cell was aimed at improving the light absorption by the middle cell, which is usually penalized in the triple configuration. In fact the front cell can absorb light at its first pass and the back cell can benefit from the reflection from the metal back contact. For this triple, the thickness of the active layers was optimized via optoelectrical modeling. The optimal device returned a PCE of 8.7%, with a small loss of V_{OC} (from 2.26 V expected to 2.20 V), and an FF of 0.66. Despite the measures to increase the current of the middle cell, the EQE was still lagging behind, resulting in a J_{SC} of 6.0 mA cm^{-2} (integrated from its EQE). By changing the middle bandgap (1.58 eV) material to PTB7-Th instead of PDPPTPT, the necessary improvement in EQE was obtained, pushing the J_{SC} up to 6.9 mA cm^{-2}. The FF was 0.68 and the V_{OC} was 2.15 V, giving an overall PCE of 10.0%.

In 2018, the first example of a solution-processed quadruple-junction solar cell with four complementary absorber layers was reported by Di Carlo Rasi et al.[68] This complex device was manufactured like the aforementioned triple-junction cell with PDCBT, PTB7-Th and PMDPP3T, by adding another back cell with an ultralow bandgap (1.1 eV): PDPPSDTPS:$PC_{60}BM$. By doing so the spectral coverage was extended up to ≈1150 nm (**Figure 12**). The diluted PEDOT:PSS/zinc oxide nanoparticles recombination layer proved to work efficiently also for this complex stack, made out of 14 functional layers, of which 11 are deposited sequentially from solutions. The V_{OC} (2.45 V) and J_{SC} (5.23 mA cm^{-2}) were matched to the expected values from modeling, and the FF was close to the expected one (0.59 instead of 0.63, respectively), corresponding to a PCE of 7.6%. The EQE spectrum of each subcell individually was accurately measured using representative light and voltage bias conditions, returning a general very good agreement with the modeled spectra. From an analysis of the optical losses, it emerged that the efficiency was mainly limited by bimolecular recombination in OPV materials, which limits the use of thick active layers to absorb more light.

Besides the series and parallel connected tandem solar cells, few studies presented new unusual device architectures. In a series connection the V_{OC}s add up and the current is determined by the current-limiting subcell, while in a parallel connection, the currents add up and the V_{OC} is close to the lowest one of the two subcells (usually the active layer with lowest bandgap). Both these factors complicate achieving high PCE values. In 2015, Guo et al. proposed a new concept to alleviate these stringent criteria,[131] by connecting in series two times the low bandgap absorber, therefore adding up their V_{OC}s, and connecting this homo tandem in parallel to the wide bandgap absorber, which has a higher V_{OC} (**Figure 13**). Going from the bottom to the top, first the low bandgap (1.46 eV) homo tandem was realized, using PDPP5T-2:$PC_{60}BM$ in the active layers. The ICL of the tandem consisted of zinc oxide/pH–neutral PEDOT:PSS, which was also used on top of the back cell. Then, silver nanowires were cast on the PEDOT:PSS film to provide the internal contact for the parallel connection. The parallel subcell was fabricated starting from zinc oxide nanoparticles on the silver nanowire layer, followed by the wide bandgap top cell of either PCDTBT:$PC_{70}BM$ (bandgap = 1.88 eV) or the commercial OPV12:$PC_{60}BM$ (bandgap = 1.73 eV), and completed by the MoO_3/Ag top electrode. The V_{OC}s of the PDPP5T-2 single cell and the PCDTBT and OPV12 subcells were as follows: 0.56,

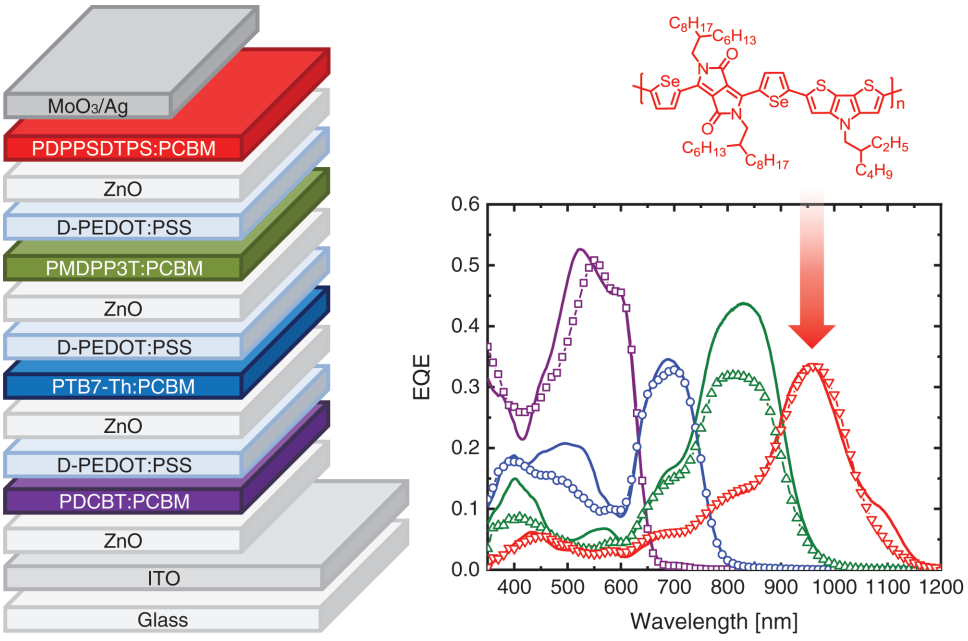

Figure 12. Quadruple-junction polymer solar cell with four complementary absorber layers and chemical structure of PDPPSDTPS. Adapted with permission.[68] Copyright 2018, The Authors. Published by Wiley-VCH.

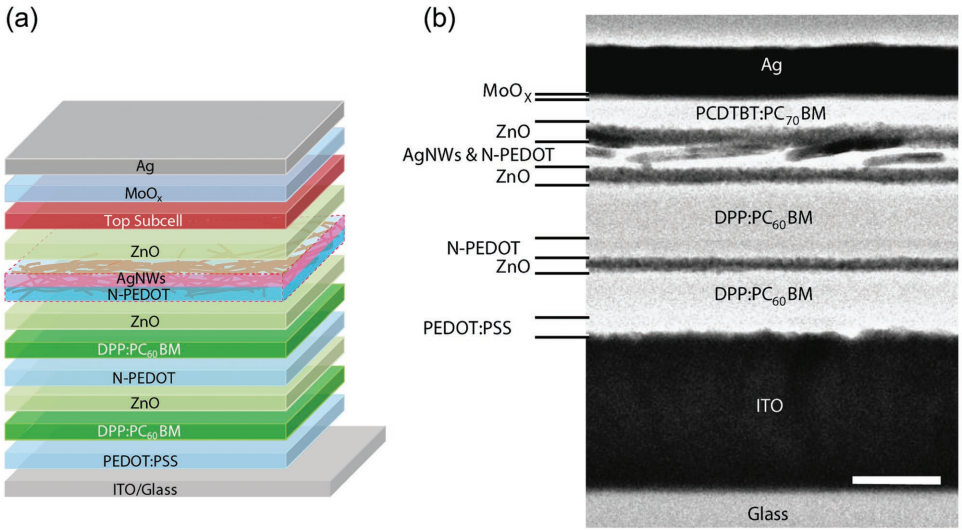

Figure 13. Series/parallel connected triple-junction cell. a) Device scheme. b) Cross-sectional transmission electron microscopy image. Scale bar is 200 nm. Reproduced with permission under the terms of the CC BY 4.0 Licence.[131] Copyright 2015, The Authors. Published by Nature Publishing Group.

0.82, and 0.77 V, respectively. The bottom homo tandem gave almost twice the V_{OC} of the PDPP5T-2 cell (1.08 V). The series-parallel solar cell demonstrated V_{OC}s of 0.89 and 0.82 V for the PCDTBT- and the OPV12-based devices, respectively. In accordance with the expectations, these values are much higher than the V_{OC} of the DPP single cell and close to the V_{OC} of the wide bandgap cells. Moreover, the J_{SC} of the subcells nicely summed up, as expected. The complete stack returned J_{SC}s of 9.67 and 9.55 mA cm^{-2}, with PCDTBT and OPV12, respectively. In both cases the PCE was 5.4%.

An overview of the relevant features of the triple- and quadruple-junction solar cells published in the covered period is collected in Table 2. Comparison with Table 1 reveals that triple and quadruple junction OPV cells have a lower PCE than the record tandem cells. The main reason that these multijunction cells do not yet outperform the best tandem or even the best single junction cells, is a lack of tailored absorber layers for triple and quadruple junction cells. To achieve record efficiency multijunction solar cells, all subcells must be able to provide high efficiencies and together provide current matching. This is more difficult to achieve for three and four layers than for two layers. Furthermore, the EQE in Figure 12 shows that for the quadruple junction solar cell the middle front, middle back, and back cell all convert photons that should have been absorbed by the previous layer in the stack. This demonstrates that at the typical layer thicknesses used (100–200 nm), the current photoactive materials are unable to absorb all light.[68] Single junction cells, and to some extent also tandem cells, are more forgiving because photons that are not absorbed in their first pass will be reflected by the metal back electrode, and can be absorbed in the second pass. For multijunction cells, these photons are more likely to be absorbed by a subsequent layer. To increase the absorption efficiency the layer thickness can be increased, but this is often accompanied by a loss in fill factor and efficiency.[68] The main reason is that bimolecular recombination increases with layer thickness, because charges use a longer trajectory before being collected and there is a higher chance for them to recombine in the active layer. The competition between extraction and recombination of free charges in OPV devices has been studied by Bartesaghi et al. who identified high charge-carrier mobilities in combination with a small Langevin prefactor as the favorable conditions for reaching high fill factors.[132] Hence, while multijunction polymer solar cells with more than two absorber layers offer the perspective of outperforming tandem cells and reaching PCEs in excess of 20%, accomplishing such goal presently hinges on developing complementary absorbing, high efficiency photoactive layers that absorb light efficiently and provide less bimolecular recombination in thick layers.

4. Characterization

4.1. EQE Measurement Under Bias

The OPV community has been actively putting a tremendous effort to increase the efficiency of solution-processed organic tandem solar cells. For a reliable development of this technology, it is important to carefully define suitable characterization methods. In this way a fair and accurate mean of comparison of the different cells is possible. These methods should account for the peculiarity of organic tandem solar cells.

The measurement of the J–V characteristics of a multijunction solar cell is performed similarly to that of single-junction cells. The EQE measurement instead, requires extra steps, due to the fact that in the ICL is usually not accessible for electrical contacts. When measuring the EQE of the tandem in the same way as for the single-junction cells, i.e., using a only monochromatic probe light of variable wavelength, the subcell absorbing less light limits the current. Under this condition, the EQE of the tandem follows the lower envelope of the EQE of the individual subcells (black squares in **Figure 14**a).[133] To measure

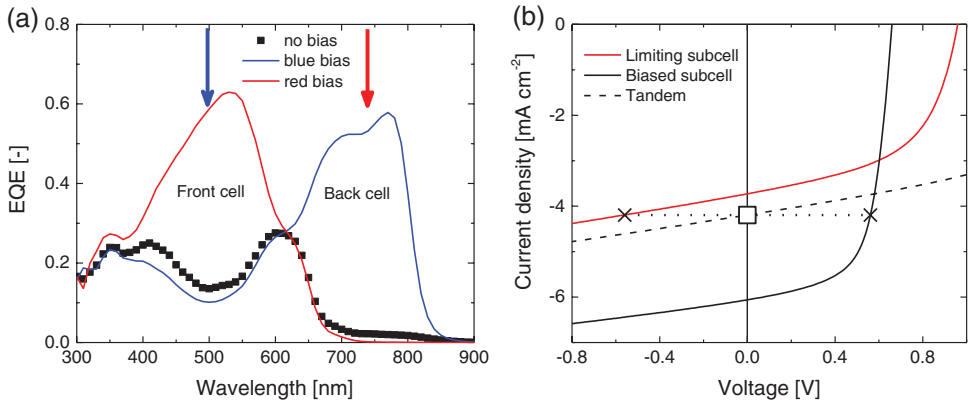

Figure 14. a) EQE spectrum of a tandem cell without light bias (black symbols) and with the addition of red or blue bias lights (arrows). b) Optically induced voltage over the limiting subcell created by the use of red bias light.

the EQE of a specific subcell over the whole spectral range, the other subcell must to be saturated by flood light, also referred to as bias light. The spectrum of this bias light should be selected according to the absorption spectrum of the subcells. By using a lock-in detection technique, the differential current response to the frequency-controlled chopped probe light provides the EQE spectrum of the nonbiased subcell (Figure 14a).

In 2010, Gilot et al. reported that for organic solar cells, the optically biased subcell generates an electric field with nonnegligible effects on the characterization.[134] In particular, while the tandem is kept at short-circuit condition, the flooded subcell is in a forward voltage bias condition and the current-limiting subcell is in a reverse voltage bias condition (Figure 14b). For most (if not all) organic solar cells this leads to overestimation of the current with respect to the short-circuit condition, due to the field dependence of the current in reverse bias. To solve this problem and obtain a correct measurement, a voltage bias correction should be applied at the terminals of the tandem during the EQE measurement with light bias. Accurate determination of this voltage correction is intricate, but according to ref. [134] the latter can be approximated as the V_{OC} of the optically biased subcell. Similar considerations can be extended to the case of solar cells with more than two junctions.

4.2. Measurement Practices and New Insights

In 2015, Timmreck et al. analyzed the characterization practices adopted in literature on OPV tandem cells from January 2009 to September 2014.[133] The alarming conclusion was that 51% of the published papers provided no EQE measurement of the subcells and no comment on the mismatch factor. 45% of the references reported the EQE measurement for the subcells but provided no comment about the mismatch factor or did not use it at all. Only the remaining 4% performed a characterization according to the standard ASTM E2236. In their publication, Timmreck et al. proposed a series of general rules for characterizing OPV tandem cells, for which we refer to ref. [133]. The rules can be summarized in four points. First, the bias lights should be selected according to the absorption spectrum of the active layer absorbers, with a special remark for homo-tandem solar cells, for which optical simulations should be involved to ensure constant biasing of one subcell all over the spectral range of measurement. Second, the necessary voltage bias (V_{bias}) should be determined, according to the expected electric field induced by the application of the light bias. For this, the V_{OC} of the single-junction solar cells can be used as approximation. Third, the spectral response measurement should be performed according to the ASTM E2236 standard test methods, using chopped monochromatic light and a lock-in technique, while applying both light and voltage bias. Fourth, the intensity of a two sources solar simulator should be adjusted to correct for the mismatch of the subcells. Under such a calibrated light source, the *J*–*V* characteristic can be measured, putting emphasis on the correct determination of the effective area of the solar cell. In addition, the authors recommended a detailed description of all the experimental procedures and setups involved in the characterization.

Herein a similar research as the one of Timmreck et al. was repeated on Web of Science, using the keywords: "TI = ((tandem OR triple* OR (multi*junction*) OR (multijunction*)) AND (organic OR polymer OR (small molecule*) OR (nonfullerene) OR (*fullerene*) OR (*fullerene-)) AND ((solar cell*) OR photovoltaic* OR (photovoltaic cell*))) AND PY = (2015–2018)," limited to the period from January 2015 to August 2018. Articles about hybrid tandem solar cells, articles where no actual device was fabricated and out-of-topic entries were excluded. From this, the papers considered "highly cited papers" were selected, repeating the research for different time periods: i) 2015–2018, ii) 2016–2018, and iii) 2017–2018. In addition, recently published papers claiming high efficiency tandems were included. The research on Web of Science returned 11 articles (13 total) in period (i), 7 (8 total) in period (ii), and 5 (6 total) in period (iii). Two entries in period (i) and one entry in periods (ii) and (iii) were excluded, being out of topic. All the entries in list (iii) overlapped with those in list (ii) and similarly for those in list (ii) with the ones in list (i). Two papers recently published[99,102] and one not covered by the keywords[97] were included because of the high efficiencies reported. Among other papers found, not covered by the keywords, one with high number of citations[131] was excluded for the high complexity of the device structure (series/parallel triple-junction cell), and the others were not considered

Table 3. Literature survey on solution-processed multijunction organic tandem solar cells in the period: January 2015 to August 2018. Please refer to the main text for a detailed description of the criteria.

EQE tandem	Light bias	V_{bias}	δJ_{SC}^{EQE} [%][a)]	Ref.
+[b)]	–	–	n.a.[c)]	[35]
+[b)]	–	–	n.a.[c)]	[65]
+	+	–	+2.2	[38]
+	+	–	+3.8	[82]
+[d)]	+	–	+4.8	[83]
+	+	–	+8.7	[84]
+	+	–	+0.7	[96]
+	+	–	+1.5	[97]
+	+	–	+3.8	[99]
+	+	–	+4.6	[104]
+	+	–	n.a.[c)]	[107]
+[d)]	+[e)]	–	+8.3	[127]
+	+	+[f)]	+8.7	[36]
+	+	+	+1.1	[102]

[a)]Relative deviation of the J_{SC} measured under solar simulator with respect to the J_{SC} from integration of the EQE spectrum of the current-limiting subcell with the reference AM1.5G solar spectrum ($^{lim}J_{SC}^{EQE}$); [b)]Homo tandem; [c)]$^{lim}J_{SC}^{EQE}$ not available; [d)]Summed EQE of the subcells exceeds 100% at some wavelengths; [e)]No details provided; [f)]No explanation of the choice.

because of a lower number of citations. Some of the characteristics of the EQE measurement there adopted were selected, and are presented in **Table 3**.

From this list of publications it appears that researchers gave greater consideration to the importance of EQE measurement. Although not always described in detail, a light bias is provided in all the references in Table 3. Two cases[35,65] where homo-tandem cells were studied, limit themselves to report the EQE measurement without any bias. Provided that leakage paths in the subcells do no contribute significantly, this should correspond to the lower envelope of the EQEs of the two subcells.[133] For what concerns the application of a voltage bias during the EQE measurement, only refs. [36] and [102] report the use of this correction, necessary to not overestimate the efficiency. Only refs. [36], [102], [104], and [127] report the mismatch factor of the subcells and only refs. [102] and [104] comment on how it was determined. Given the fact that in a series-connected tandem solar cell the current is limited by the subcell generating less current, it is interesting to compare the J_{SC} of the tandem measured under simulated solar radiation (AM1.5G spectrum) with the J_{SC} of the current-limiting subcell ($^{lim}J_{SC}^{EQE}$). The latter can be derived from its corresponding EQE spectrum, integrated with the tabulated reference AM1.5G solar spectrum. In Table 3, the relative deviations between J_{SC} and $^{lim}J_{SC}^{EQE}$ is indicated with δJ_{SC}^{EQE}. Another easy operation for a quick check that gives more information about the EQE measurement consists in adding up the EQEs of the individual subcells. Although this in not always done in this sample of literature, we note that in refs. [83] and [127] the summed EQE locally exceeds 100%. No comment was given on possible reasons for this unexpected outcome.

Timmreck et al. provided a rigorous method to accurately determine the efficiency of OPV devices.[132] Possibly due to the limited experimental availability and/or the intricate nature of some of the steps enumerated, the application of this vade mecum is never fully rigorously performed (following the sensible sample of the recent literature here considered). Nevertheless, what discussed in this section about the EQE measurement can likely improve the accuracy, without introducing experimental complications. In particular, 1) the usage of the proper voltage bias (or the readily available V_{OC} of the single-junction cells as approximation), 2) the comparison of the J_{SC} of the tandem as measured under simulated solar radiation with the EQE-integrated J_{SC} of the current-limiting subcell, and 3) adding up the EQEs of the subcells over the spectral range of measurement.

Concerning homo-tandem solar cells, Bahro et al. addressed the problem of measuring the individual subcells by using an intermediate electrode in the ICL zone.[135] In their study, they fabricated homo tandems based on PTB7:$PC_{70}BM$ as active layer. A combination of modified PEDOT:PSS and ZnO nanoparticles was involved as ICL. For the creation of the intermediate electrode, another formulation of highly conductive PEDOT:PSS was deposited before the ICL on top of the front cell, and structured laterally to avoid effects due to its high lateral conductivity. The thickness of the PEDOT:PSS bilayer in the three-terminal device was controlled to match the one in the reference two-terminal tandem, without the extra PEDOT:PSS electrode. The authors showed that the ICL based on the extra electrode implied no difference in the optoelectronic performance of the device. Therefore, the EQE of both front and back subcells could be directly measured, by simply contacting the intermediate electrode.

In 2017 Di Carlo Rasi et al. published a characterization protocol for triple-junction polymer solar cells.[136] The triple was the same already presented in Section 2.2 from ref. [67], with PDCBT, PTB7-Th and PMDPP3T blended with PCBM as front, middle, and back subcells, respectively. Besides the measurement of its J–V characteristic curve, the focus was given on the EQE measurement of each individual subcell. The latter was isolated and acquired by optically biasing the other two subcells. For the purpose, high power light-emitting diodes with wavelength (in nm) of 530, 730, and 940 nm were used, which matched the absorption spectra of the subcells. By performing optical modeling calculations, the amount of current generated by each subcell under different (combinations of) light bias was predicted. Due to the partial spectral overlap, this was aimed at ensuring with enough confidence that only one subcell is current-limiting over the whole range of wavelengths of the measurement. In this prediction, the different IQEs of the subcells were taken into account. In addition, the predicted light intensity experienced by the subcells under light bias was recreated on single-junction cells representative of the subcells and their J–V characteristic was measured. In this way, the necessary voltage bias correction was determined for each subcell. Without this correction, the EQE of the subcells was seen to substantially overestimate the correct EQE. The measured EQEs matched remarkably well the predicted spectra via optoelectrical modeling, validating the whole procedure. In 2018, the same group demonstrated that the protocol could be extended

to characterize a device with higher complexity: a quadruple-junction polymer solar cell.[68]

Concerning the ICL, Prosa et al. proposed a combination of two measurement techniques to identify the source of minor electrical losses.[137] For the purpose, representative single-junction cells were fabricated, in which the whole ICL stack is sandwiched between the ITO electrode and the photoactive layer. The first technique consists in determining the photocurrent versus bias voltage (J_{ph}–V) curve. Above V_{OC} (injection regime), there is the so-called compensation voltage V_0, where $J_{ph} = J_{dark}$, J_{dark} being the current density in the dark. The authors show how at $V > V_0$ the blocking capacity of the interlayer (of the ICL) in contact with the active layer can be evaluated from the behavior of J_{ph}. On the other hand, individuation of injection barriers in the same transport layer is obtained by means of electroluminescence measurements. The approach shows minor losses at the ICL which could be hardly detectable from the standard measurement of the J–V characteristic curve of the representative subcell of the tandem, but which could be relevant in the photovoltaic performance of the complete tandem device.

5. Use of Multijunction Polymer Solar Cells

Besides the clear interest in increasing the power conversion efficiency over that of single-junction devices, specific applications can be identified where the properties of OPV tandem cells turn advantageous. Photoelectrochemical water splitting is one of them, because OPV tandem cells can provide the necessary voltage at the operating point. This voltage should exceed the standard potential of $E^0_{H2O} = 1.23$ V for the water splitting reaction plus the overpotentials at the electrodes. Another application reported is the use of tandem polymer solar cells as photodiodes for future integration in artificial retinal implants.

The standard potential for water splitting is $E^0_{H2O} = 1.23$ V, which in practice is further increased to 1.4–1.8 V due to overpotentials for oxygen/hydrogen formation at the electrodes. Provided that enough operating voltage is delivered by the solar cell, there is a direct proportionality between photocurrent and hydrogen evolution. Assuming 100% Faradaic efficiency, the solar-to-hydrogen evolution efficiency (η_{STH}) follows the relation $\eta_{STH} = J_{op} \times E^0_{H2O}/P_{in}$, where J_{op} is the operating current density delivered by the cell during water splitting. Preferably the cell and electrode materials are designed in such a way that the cell operates in its maximum power point, i.e., $J_{op} = J_{max}$ and $V_{op} = V_{max}$, in which case $\eta_{STH} = PCE \times (E^0_{H2O}/V_{op})$. In 2013, Esiner et al. demonstrated the possibility of using triple-junction solar cells for water splitting.[24] In 2015 Esiner et al. used a more efficient triple-junction solar cell for photoelectrochemical water splitting, comprising PCDTBT:$PC_{70}BM$ as wide bandgap front cell and PMDPP3T:$PC_{60}BM$ as both middle and back cells.[129] The interconnection of the subcells was realized with ZnO nanoparticles and pH–neutral PEDOT:PSS (**Figure 15**a). The study shed light on the effect of the nature and surface area of the catalyst connected to a triple-junction cell on the η_{STH} efficiency. In particular, a η_{STH} of 5.4% was obtained with RuO_2-coated Ti substrates as catalysts for both hydrogen and oxygen evolution, with a surface area 18 times the one of the solar cell used. They also fabricated a water splitting device by replacing the RuO_2 catalyst by the earth-abundant Co_3O_4/NiMoZn catalysts, which yielded a η_{STH} of 4.9%. When the surface area of the catalyst was reduced to ≈0.7 times the area of the solar cell, the higher current density in the catalyst caused an increase in overpotential, which shifted the operating voltage V_{op} from 1.49 to 1.69 V, i.e., away from the maximum power point of the solar cell. Consequently, η_{STH} decreased to 3.6%. Because the photon flux is distributed over only two instead of three absorber layers a tandem solar cell can generate a higher current density than a triple-junction cell at the same optical bandgap. Hence, provided that the required operating voltage can be reached, a tandem cell can provide a high η_{STH}. Figure 15b shows a wireless artificial leaf in which the triple junction solar cell is integrated with RuO_2 catalysts electrodeposited on the ITO contacts. In 2016, Esiner et al. reported a wide bandgap donor polymer containing a pentacyclic lactam unit, PTPTIBDT-OD.[138] The optical bandgap of this material is 2.04 eV and in combination with $PC_{70}BM$ as acceptor it can

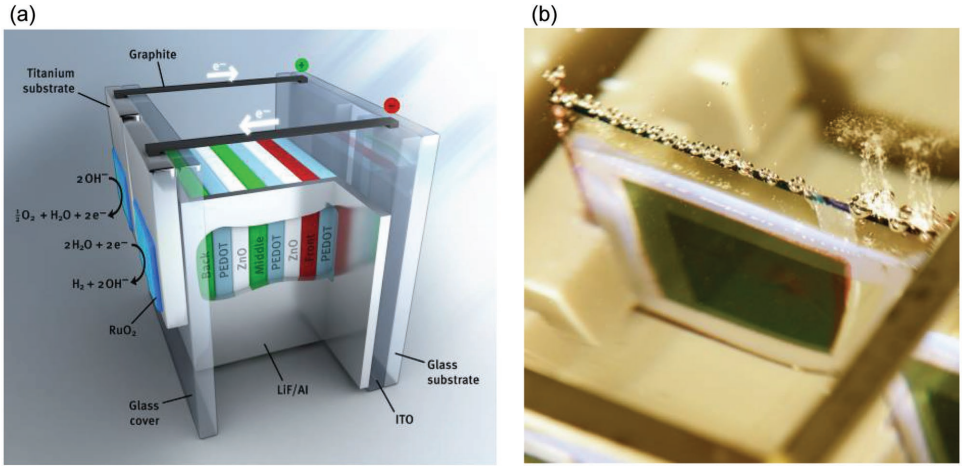

Figure 15. Integrated triple-junction polymer solar cell/RuO_2 catalysts for photoelectrochemical water splitting. Device scheme a) and real device under operating conditions b). Reproduced with permission under the terms of the CC BY 3.0 Licence.[129] Copyright 2015, The Authors. Published by The Royal Society of Chemistry.

afford a V_{OC} of 0.90 V in a single-junction solar cell. This active layer was used for both the front and back subcells of a homo-tandem device. To avoid voltage losses, the ICL was carefully designed using a ZnO/pH–neutral PEDOT:PSS/MoO_3 stack, allowing a V_{OC} of 1.74 V. For the water splitting reaction, the authors connected the solar cell to a RuO_2-coated Ti substrate catalytic electrode for oxygen and hydrogen evolution or a Pt plate catalyst for hydrogen evolution, in a KOH solution. The operating voltage for water splitting of this system was 1.5 V. In virtue of the high fill factor of 0.73 for this tandem, an η_{STH} of 4.3% could be achieved, assuming 100% Faradaic efficiency. Also in 2016, Gao et al. reported a homo-tandem polymer solar cell adopting PBDTTPD as a wide bandgap donor material in combination with $PC_{70}BM$.[128] This donor material has a bandgap of 1.85 eV and can deliver a V_{OC} of 0.92 V in a single-junction device, together with an internal quantum efficiency (IQE) around 0.9. The homo tandem affords J_{op} = 5.4 mA cm^{-2} during water splitting at V_{op} = 1.5 V, using an aqueous NaOH solution and platinum and nickel foam for hydrogen and oxygen evolution electrodes, respectively. The cell thus affords η_{STH} of 6.6% when assuming 100% Faradaic efficiency. In the same year, Elias et al. presented a homo-triple junction for water splitting, i.e., using the same absorber in all the three subcells, PTB7:$PC_{70}BM$.[130] The structure of this device was inverted, with the successful MoO_3/Ag/PFN stack as ICL. The triple was characterized by a V_{OC} of 2.13 V, which together with an outstanding FF of 0.76 (certainly considering the number of layers in the stack) ensured a high value of J_{op}. A 6% in η_{STH} was achieved at neutral pH, by connecting the triple cell to a cathode of NiMoZn on stainless steel and an anode of RuO_2 on glassy carbon. The choice of the catalysts is particularly valuable since the first one is made of relatively abundant materials and the second one was manufactured with a minimal content of RuO_2. As already addressed before, polymer blends with non-fullerene acceptors can provide in general significantly higher V_{OC}s than fullerene-based cells. In 2016 Liu et al.[94] and in 2017 Chen et al.[65] reported V_{OC}s of 1.97 and 2.16 V for these two NFA-based tandem cells, respectively, and demonstrated the evolution of gasses at the catalytic electrodes (platinum and nickel foam in a NaOH solution).

Another possible application of polymer tandem cells was recently described by Simone et al.[139] The authors evaluated the potential of organic photodiodes (OPDs) sensitive to near-infrared light for integration in a retinal prosthesis. These photodiodes are practically equivalent to tandem polymer solar cells, and they should be arranged in an array integrated in the retinal prosthesis. The concept, illustrated in **Figure 16**, involves illumination of the OPDs with pulsed near-infrared light via a projection system included in wearable glasses. Each OPD pixel delivers a consequential pulsed photocurrent to nearby neural cells in the retinal network by means of stimulating microelectrodes. This idea is inspired on the work published by Mathieson et al.,[140] where the retinal implant was based on series-connected silicon photodiodes lying on the same surface. The potential advantage of having an OPD pixels array is that this one may be processed on ultrathin plastic foil, resulting in a mechanically flexible, softer implant. The additional advantage is represented by the fact that the series-connected cells are piled on each other, allowing for higher pixel density and in turns the resolution. The electrical charge photogenerated by tandem OPDs under pulsed monochromatic light centered at 830 nm reached typical neural stimulation levels at physiologically safe intensities. This demonstrates the viability of high-resolution retinal prostheses based on tandem OPD arrays.

6. Conclusions

The results reported in this review point toward a very active research community on solution-processed multijunction organic solar cells. The top efficiency for tandems with polymer:NFA photoactive blends reached a PCE of 17.4%, and for tandems featuring small molecular donors blended with PCBM the highest PCE is 12.5%. Worth to mention is the PCE of 15% for hybrid evaporated small molecules (front cell) and solution-processed (back cell) tandems. Also all-polymer tandem cells underwent a significant improvement of the performance up to 11.2% despite a small number of investigations addressing these cells. Polymer:PCBM-based tandems were reported multiple times capable of PCE >11%. The PTB7-Th donor was adopted in many cases of efficient tandem solar cells, irrespective of whether PCBM and/or NFAs were blended with it. In addition to the high efficiency,

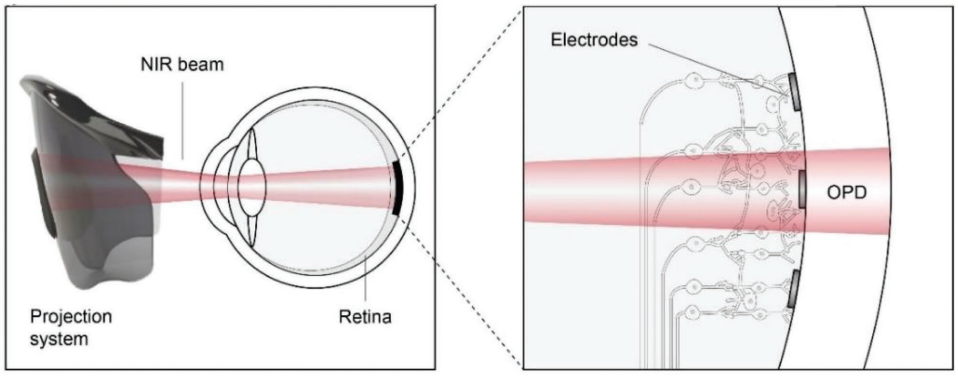

Figure 16. Concept of application of organic near-infrared photodiodes for artificial retinal implant adopted by Simone et al.,[139] inspired by the work of Mathieson et al.[140] Reproduced with permission.[139] Copyright 2018, The Authors. Published by Wiley-VCH.

the high V_{OC} (especially of NFA systems) make OPV tandems suitable for photoelectrochemical water splitting application. From the point of view of the ICL, PEDOT:PSS and ZnO nanoparticles are still widely used in research, with interesting developments to improve their processing. A significant focus lied on the use of conjugated polyelectrolytes charge transport layers in the ICL. Among these, the use of PFN was reported by multiple groups, especially in the stack: MoO_3/Ag/PFN. The latter allowed achieving high FF values as well as an intriguing solution to tune the optical electric field in the device, improving the balance of photocurrent in the subcells. The thickness-dependent performance of single-junction cells, deriving from bimolecular recombination, was tackled in some papers by adopting the same absorber system in a homotandem solar cell, demonstrating improved absorption of light, accompanied by an increase in efficiency. Triple-junction solar cells were developed in a limited number of studies due to their intricate requirements in terms of current matching and more elaborate processing and characterization. Nevertheless, even a quadruple-junction polymer solar cell with complementary absorber layers was demonstrated. At present, the performance of triple- and quadruple-junction cells is less than the best single-junction and tandem cells. The main reason is the bimolecular recombination in the thick absorber layers that are needed. If bimolecular recombination can be reduced, PCEs exceeding those of the best tandem cells are feasible for multijunctions. A critical analysis on the procedure to follow to correctly characterize OPV tandems was presented in the early 2015. So far, a few relevant papers followed the guidelines rigorously, but the awareness of correct characterization has certainly been increased in recent years. In view of the high efficiencies now reported, the currently available studies on stability and on upscaling the technology should be continued, to meet the requirements for industrial manufacturing and reaching the market.

Acknowledgements

The authors thank Bart van Overbeeke, the ICMS animation studio, and Dario Simone for providing artwork. The authors acknowledge funding from the European Research Council under the European Union's Seventh Framework Programme (FP/2007-2013)/ERC Grant Agreement No. 339031. The research also received funding from the Ministry of Education, Culture and Science (Gravity program 024.001.035).

Conflict of Interest

The authors declare no conflict of interest.

Keywords

multijunction solar cells, organic semiconductors, organic solar cells, photovoltaics, tandem solar cells

Received: October 8, 2018
Revised: November 7, 2018
Published online: December 27, 2018

[1] S. Zhang, Y. Qin, J. Zhu, J. Hou, *Adv. Mater.* **2018**, *30*, 1800868.
[2] Z. Zheng, Q. Hu, S. Zhang, D. Zhang, J. Wang, S. Xie, R. Wang, Y. Qin, W. Li, L. Hong, N. Liang, F. Liu, Y. Zhang, Z. Wei, Z. Tang, T. P. Russell, J. Hou, H. Zhou, *Adv. Mater.* **2018**, *30*, 1801801.
[3] S. Li, L. Ye, W. Zhao, H. Yan, B. Yang, D. Liu, W. Li, H. Ade, J. Hou, *J. Am. Chem. Soc.* **2018**, *140*, 7159.
[4] W. Shockley, H. J. Queisser, *J. Appl. Phys.* **1961**, *32*, 510.
[5] S. Rühle, *Sol. Energy* **2016**, *130*, 139.
[6] A. De Vos, *J. Phys. D: Appl. Phys.* **1980**, *13*, 839.
[7] M. Hiramoto, M. Suezaki, M. Yokoyama, *Chem. Lett.* **1990**, *19*, 327.
[8] A. Yakimov, S. R. Forrest, *Appl. Phys. Lett.* **2002**, *80*, 1667.
[9] K. Triyana, T. Yasuda, K. Fujita, T. Tsutsui, *Jpn. J. Appl. Phys.* **2004**, *43*, 2352.
[10] J. Drechsel, B. Männig, F. Kozlowski, D. Gebeyehu, A. Werner, M. Koch, K. Leo, M. Pfeiffer, *Thin Solid Films* **2004**, *451–452*, 515.
[11] B. Maennig, J. Drechsel, D. Gebeyehu, P. Simon, F. Kozlowski, A. Werner, F. Li, S. Grundmann, S. Sonntag, M. Koch, K. Leo, M. Pfeiffer, H. Hoppe, D. Meissner, N. S. Sariciftci, I. Riedel, V. Dyakonov, J. Parisi, *Appl. Phys. A* **2004**, *79*, 1.
[12] J. Gilot, M. M. Wienk, R. A. J. Janssen, *Appl. Phys. Lett.* **2007**, *90*, 143512.
[13] J. Y. Kim, K. Lee, N. E. Coates, D. Moses, T.-Q. Nguyen, M. Dante, A. J. Heeger, *Science* **2007**, *317*, 222.
[14] J. Gilot, M. M. Wienk, R. A. J. Janssen, *Adv. Mater.* **2010**, *22*, E67.
[15] L. Dou, J. You, J. Yang, C.-C. Chen, Y. He, S. Murase, T. Moriarty, K. Emery, G. Li, Y. Yang, *Nat. Photonics* **2012**, *6*, 180.
[16] J. You, L. Dou, K. Yoshimura, T. Kato, K. Ohya, T. Moriarty, K. Emery, C.-C. Chen, J. Gao, G. Li, Y. Yang, *Nat. Commun.* **2013**, *4*, 1446.
[17] C.-H. Chou, W. L. Kwan, Z. Hong, L.-M. Chen, Y. Yang, *Adv. Mater.* **2011**, *23*, 1282.
[18] Y. Zhou, C. Fuentes-Hernandez, J. W. Shim, T. M. Khan, B. Kippelen, *Energy Environ. Sci.* **2012**, *5*, 9827.
[19] J. Jo, J.-R. Pouliot, D. Wynands, S. D. Collins, J. Y. Kim, T. L. Nguyen, H. Y. Woo, Y. Sun, M. Leclerc, A. J. Heeger, *Adv. Mater.* **2013**, *25*, 4783.
[20] D. W. Zhao, X. W. Sun, C. Y. Jiang, A. K. K. Kyaw, G. Q. Lo, D. L. Kwong, *IEEE Electron Device Lett.* **2009**, *30*, 490.
[21] Y. Zou, Z. Deng, W. J. Potscavage, M. Hirade, Y. Zheng, C. Adachi, *Appl. Phys. Lett.* **2012**, *100*, 243302.
[22] J. Gilot, *Ph.D. Thesis*, Eindhoven University of Technology **2010**.
[23] Press release by Heliatek (February **2016**), http://heliatek.com (accessed: October 2018).
[24] S. Esiner, H. Van Eersel, M. M. Wienk, R. A. J. Janssen, *Adv. Mater.* **2013**, *25*, 2932.
[25] W. Li, A. Furlan, K. H. Hendriks, M. M. Wienk, R. A. J. Janssen, *J. Am. Chem. Soc.* **2013**, *135*, 5529.
[26] C.-C. Chen, W.-H. Chang, K. Yoshimura, K. Ohya, J. You, J. Gao, Z. Hong, Y. Yang, *Adv. Mater.* **2014**, *26*, 5670.
[27] A. Furlan, R. A. J. Janssen, *RSC Polym. Chem. Ser.* **2016**, *17*, 310.
[28] Z. Hong, L. Dou, G. Li, Y. Yang, *Top. Appl. Phys.* **2015**, *130*, 315.
[29] N. Li, T. Ameri, C. J. Brabec, in *Organic Solar Cells* (Ed. Q. Qiao) CRC Press, Boca Raton, FL **2015**, Ch. 12, pp. 337–377.
[30] O. Adebanjo, B. Vaagensmith, Q. Qiao, *J. Mater. Chem. A* **2014**, *2*, 10331.
[31] K. Glaser, A. Puetz, J. Mescher, D. Bahro, A. Colsmann, in *Organic Photovoltaics*, 2nd ed. (Eds. J. C Brabec, U. Scherf, V. Dyakonov), Wiley-VCH, Weinheim, Germany **2014**, Ch. 14, pp. 445–463.
[32] J. You, L. Dou, Z. Hong, G. Li, Y. Yang, *Prog. Polym. Sci.* **2013**, *38*, 1909.
[33] T. Ameri, N. Li, C. J. Brabec, *Energy Environ. Sci.* **2013**, *6*, 2390.
[34] T. Ameri, G. Dennler, C. Lungenschmied, C. J. Brabec, *Energy Environ. Sci.* **2009**, *2*, 347.
[35] H. Zhou, Y. Zhang, C.-K. Mai, S. D. Collins, G. C. Bazan, T.-Q. Nguyen, A. J. Heeger, *Adv. Mater.* **2015**, *27*, 1767.

[36] Y. Cui, H. Yao, B. Gao, Y. Qin, S. Zhang, B. Yang, C. He, B. Xu, J. Hou, *J. Am. Chem. Soc.* **2017**, *139*, 7302.
[37] J. Lee, H. Kang, S. Kee, S. H. Lee, S. Y. Jeong, G. Kim, J. Kim, S. Hong, H. Back, K. Lee, *ACS Appl. Mater. Interfaces* **2016**, *8*, 6144.
[38] K. Zhang, K. Gao, R. Xia, Z. Wu, C. Sun, J. Cao, L. Qian, W. Li, S. Liu, F. Huang, X. Peng, L. Ding, H.-L. Yip, Y. Cao, *Adv. Mater.* **2016**, *28*, 4817.
[39] K. Zhang, B. Fan, R. Xia, X. Liu, Z. Hu, H. Gu, S. Liu, H.-L. Yip, L. Ying, F. Huang, Y. Cao, *Adv. Energy Mater.* **2018**, *8*, 1703180.
[40] K. Zhang, R. Xia, B. Fan, X. Liu, Z. Wang, S. Dong, H.-L. Yip, L. Ying, F. Huang, Y. Cao, *Adv. Mater.* **2018**, *30*, 1803166.
[41] L. Zuo, C.-Y. Chang, C.-C. Chueh, S. Zhang, H. Li, A. K.-Y. Jen, H. Chen, *Energy Environ. Sci.* **2015**, *8*, 1712.
[42] A. Martínez-Otero, Q. Liu, P. Mantilla-Perez, M. M. Bajo, J. Martorell, *J. Mater. Chem. A* **2015**, *3*, 10681.
[43] S. Lu, X. Guan, X. Li, W. E. I. Sha, F. Xie, H. Liu, J. Wang, F. Huang, W. C. H. Choy, *Adv. Energy Mater.* **2015**, *5*, 1500631.
[44] D. W. Zhao, L. Ke, Y. Li, S. T. Tan, A. K. K. Kyaw, H. V. Demir, X. W. Sun, D. L. Carroll, G. Q. Lo, D. L. Kwong, *Solar Energy Mater. Solar Cells* **2011**, *95*, 921.
[45] S. Bag, R. J. Patel, A. Bunha, C. Grand, J. D. Berrigan, M. J. Dalton, B. J. Leever, J. R. Reynolds, M. F. Durstock, *ACS Appl. Mater. Interfaces* **2016**, *8*, 16.
[46] T. Becker, S. Trost, A. Behrendt, I. Shutsko, A. Polywka, P. Görrn, P. Reckers, C. Das, T. Mayer, D. Di Carlo Rasi, K. H. Hendriks, M. M. Wienk, R. A. J. Janssen, T. Riedl, *Adv. Energy Mater.* **2018**, *8*, 1702533.
[47] F. Verbakel, S. C. J. Meskers, R. A. J. Janssen, *Appl. Phys. Lett.* **2006**, *89*, 102103.
[48] D. Di Carlo Rasi, P. M. J. G. van Thiel, H. Bin, K. H. Hendriks, G. H. L. Heintges, M. M. Wienk, R. A. J. Janssen, unpublished.
[49] A. F. Mitul, L. Mohammad, S. Venkatesan, N. Adhikari, S. Sigdel, Q. Wang, A. Dubey, D. Khatiwada, Q. Qiao, *Nano Energy* **2015**, *11*, 56.
[50] X. Du, O. Lytken, M. S. Killian, J. Cao, T. Stubhan, M. Turbiez, P. Schmuki, H.-P. Steinrück, L. Ding, R. H. Fink, N. Li, C. J. Brabec, *Adv. Energy Mater.* **2017**, *7*, 1601959.
[51] N. Torabi, A. Behjat, M. Shahpari, S. Edalati, *J. Nanophotonics* **2015**, *9*, 093049.
[52] M. Raïssi, S. Vedraine, R. Garuz, T. Trigaud, B. Ratier, *Solar Energy Mater. Solar Cells* **2017**, *160*, 494.
[53] S. Lu, X. Guan, X. Li, J. Liu, F. Huang, W. C. H. Choy, *Nano Energy* **2016**, *21*, 123.
[54] S.-Y. Chang, Y.-C. Lin, P. Sun, Y.-T. Hsieh, L. Meng, S.-H. Bae, Y.-W. Su, W. Huang, C. Zhu, G. Li, K.-H. Wei, Y. Yang, *Sol. RRL* **2017**, *1*, 1700139.
[55] Z. Shi, H. Liu, L. Xia, Y. Bai, F. Wang, B. Zhang, T. Hayat, A. Alsaedi, Z. Tan, *Chin. J. Chem.* **2018**, *36*, 194.
[56] S. Lu, H. Lin, S. Zhang, J. Hou, W. C. H. Choy, *Adv. Energy Mater.* **2017**, *7*, 1701164.
[57] M. Vasilopoulou, E. Polydorou, A. M. Douvas, L. C. Palilis, S. Kennou, P. Argitis, *Energy Environ. Sci.* **2015**, *8*, 2448.
[58] C.-Y. Chang, W.-K. Huang, Y.-C. Chang, K.-T. Lee, H.-Y. Siao, *Chem. Mater.* **2015**, *27*, 1869.
[59] W. J. da Silva, F. K. Schneider, A. R. bin Mohd Yusoff, J. Jang, *Sci. Rep.* **2016**, *5*, 18090.
[60] M. Raïssi, L. Vignau, E. Cloutet, B. Ratier, *Org. Electron.* **2015**, *21*, 86.
[61] R. Kang, S. Park, Y. K. Jung, D. C. Lim, M. J. Cha, J. H. Seo, S. Cho, *Adv. Energy Mater.* **2018**, *8*, 1702165.
[62] H. Kang, S. Kee, K. Yu, J. Lee, G. Kim, J. Kim, J.-R. Kim, J. Kong, K. Lee, *Adv. Mater.* **2015**, *27*, 1408.
[63] S. Kim, H. Kang, S. Hong, J. Lee, S. Lee, B. Park, J. Kim, K. Lee, *Adv. Funct. Mater.* **2016**, *26*, 3563.
[64] Q. Wei, T. Nishizawa, K. Tajima, K. Hashimoto, *Adv. Mater.* **2008**, *20*, 2211.
[65] S. Chen, G. Zhang, J. Liu, H. Yao, J. Zhang, T. Ma, Z. Li, H. Yan, *Adv. Mater.* **2017**, *29*, 1604231.
[66] M. Prosa, M. Tessarolo, M. Bolognesi, T. Cramer, Z. Chen, A. Facchetti, B. Fraboni, M. Seri, G. Ruani, M. Muccini, *Adv. Mater. Interfaces* **2016**, *3*, 1600770.
[67] D. Di Carlo Rasi, K. H. Hendriks, G. H. L. Heintges, G. Simone, G. H. Gelinck, V. S. Gevaerts, R. Andriessen, G. Pirotte, W. Maes, W. Li, M. M. Wienk, R. A. J. Janssen, *Sol. RRL* **2018**, *2*, 1800018.
[68] D. Di Carlo Rasi, K. H. Hendriks, M. M. Wienk, R. A. J. Janssen, *Adv. Mater.* **2018**, *30*, 1803836.
[69] Y. Ka, H. Hwang, C. Kim, *Sci. Rep.* **2017**, *7*, 1942.
[70] Y. Ka, H. Kim, S. Han, C. Kim, *Nanoscale* **2018**, *10*, 12588.
[71] X. Che, Y. Li, Y. Qu, S. R. Forrest, *Nat. Energy* **2018**, *3*, 422.
[72] S. Lee, T. E. Kang, D. Han, H. Kim, B. J. Kim, J. Lee, S. Yoo, *Solar Energy Mater. Solar Cells* **2015**, *137*, 34.
[73] L. Zuo, J. Yu, X. Shi, F. Lin, W. Tang, A. K.-Y. Jen, *Adv. Mater.* **2017**, *29*, 1702547.
[74] P. Mantilla-Perez, A. Martinez-Otero, P. Romero-Gomez, J. Martorell, *ACS Appl. Mater. Interfaces* **2015**, *7*, 18435.
[75] L. Zuo, C.-Y. Chang, C.-C. Chueh, Y. Xu, H. Chen, A. K.-Y. Jen, *J. Mater. Chem. A* **2016**, *4*, 961.
[76] J. A. Mayer, T. Offermans, M. Chrapa, M. Pfannmöller, S. Bals, R. Ferrini, G. Nisato, *Opt. Express* **2018**, *26*, A240.
[77] A. Mertens, J. Mescher, D. Bahro, M. Koppitz, A. Colsmann, *Opt. Express* **2016**, *24*, A898.
[78] M. Riede, C. Uhrich, J. Widmer, R. Timmreck, D. Wynands, G. Schwartz, W.-M. Gnehr, D. Hildebrandt, A. Weiss, J. Hwang, S. Sundarraj, P. Erk, M. Pfeiffer, K. Leo, *Adv. Funct. Mater.* **2011**, *21*, 3019.
[79] B. Luo, Y. Jiang, L. Mao, W. Meng, F. Jiang, Y. Xu, Y. Zhou, *J. Mater. Chem. C* **2017**, *5*, 7884.
[80] S.-H. Liao, H.-J. Jhuo, P.-N. Yeh, Y.-S. Cheng, Y.-L. Li, Y.-H. Lee, S. Sharma, S.-A. Chen, *Sci. Rep.* **2015**, *4*, 6813.
[81] Q. Zhang, X. Wan, F. Liu, B. Kan, M. Li, H. Feng, H. Zhang, T. P. Russell, Y. Chen, *Adv. Mater.* **2016**, *28*, 7008.
[82] Y. Ma, S.-C. Chen, Z. Wang, W. Ma, J. Wang, Z. Yin, C. Tang, D. Cai, Q. Zheng, *Nano Energy* **2017**, *33*, 313.
[83] Z. Zheng, S. Zhang, M. Zhang, K. Zhao, L. Ye, Y. Chen, B. Yang, J. Hou, *Adv. Mater.* **2015**, *27*, 1189.
[84] Z. Zheng, S. Zhang, J. Zhang, Y. Qin, W. Li, R. Yu, Z. Wei, J. Hou, *Adv. Mater.* **2016**, *28*, 5133.
[85] W. Li, K. H. Hendriks, A. Furlan, W. S. C. Roelofs, M. M. Wienk, R. A. J. Janssen, *J. Am. Chem. Soc.* **2013**, *135*, 18942.
[86] C. Duan, A. Furlan, J. J. van Franeker, R. E. M. Willems, M. M. Wienk, R. A. J. Janssen, *Adv. Mater.* **2015**, *27*, 4461.
[87] B. Guo, X. Guo, W. Li, X. Meng, W. Ma, M. Zhang, Y. Li, *J. Mater. Chem. A* **2016**, *4*, 13251.
[88] S. Song, K. Kranthiraja, J. Heo, T. Kim, B. Walker, S.-H. H. Jin, J. Y. Kim, *Adv. Energy Mater.* **2017**, *7*, 1700782.
[89] J. Hou, O. Inganäs, R. H. Friend, F. Gao, *Nat. Mater.* **2018**, *17*, 119.
[90] P. Cheng, G. Li, X. Zhan, Y. Yang, *Nat. Photonics* **2018**, *12*, 131.
[91] A. Wadsworth, M. Moser, A. Marks, M. S. Little, N. Gasparini, C. J. Brabec, D. Baran, I. McCulloch, *Chem. Soc. Rev.* **2018**, https://doi.org/10.1039/C7CS00892A.
[92] G. Zhang, J. Zhao, P. C. Y. Chow, K. Jiang, J. Zhang, Z. Zhu, J. Zhang, F. Huang, H. Yan, *Chem. Rev.* **2018**, *118*, 3447.
[93] J. Liu, S. Chen, D. Qian, B. Gautam, G. Yang, J. Zhao, J. Bergqvist, F. Zhang, W. Ma, H. Ade, O. Inganäs, K. Gundogdu, F. Gao, H. Yan, *Nat. Energy* **2016**, *1*, 16089.
[94] W. Liu, S. Li, J. Huang, S. Yang, J. Chen, L. Zuo, M. Shi, X. Zhan, C.-Z. Li, H. Chen, *Adv. Mater.* **2016**, *28*, 9729.
[95] X. Shi, L. Zuo, S. B. Jo, K. Gao, F. Lin, F. Liu, A. K.-Y. Jen, *Chem. Mater.* **2017**, *29*, 8369.

[96] Y. Qin, Y. Chen, Y. Cui, S. Zhang, H. Yao, J. Huang, W. Li, Z. Zheng, J. Hou, *Adv. Mater.* **2017**, *29*, 1606340.
[97] Y. Cui, H. Yao, C. Yang, S. Zhang, J. Hou, *Acta Polym. Sin.* **2018**, *2*, 223.
[98] Z. Shi, H. Liu, J. Li, F. Wang, Y. Bai, X. Bian, B. Zhang, A. Alsaedi, T. Hayat, Z. Tan, *Solar Energy Mater. Solar Cells* **2018**, *180*, 1.
[99] Y. Zhang, B. Kan, Y. Sun, Y. Wang, R. Xia, X. Ke, Y.-Q.-Q. Yi, C. Li, H.-L. Yip, X. Wan, Y. Cao, Y. Chen, *Adv. Mater.* **2018**, *30*, 1707508.
[100] Q. Yue, Z. Zhou, S. Xu, J. Zhang, X. Zhu, *J. Mater. Chem. A* **2018**, *6*, 13588.
[101] X. Xu, T. Yu, Z. Bi, W. Ma, Y. Li, Q. Peng, *Adv. Mater.* **2018**, *30*, 1703973.
[102] L. Meng, Y. Zhang, X. Wan, C. Li, X. Zhang, Y. Wang, X. Ke, Z. Xiao, L. Ding, R. Xia, H.-L. Yip, Y. Cao, Y. Chen, *Science* **2018**, *361*, 1094.
[103] J.-H. Kim, J. B. Park, H. Yang, I. H. Jung, S. C. Yoon, D. Kim, D.-H. Hwang, *ACS Appl. Mater. Interfaces* **2015**, *7*, 23866.
[104] M. Li, K. Gao, X. Wan, Q. Zhang, B. Kan, R. Xia, F. Liu, X. Yang, H. Feng, W. Ni, Y. Wang, J. Peng, H. Zhang, Z. Liang, H.-L. Yip, X. Peng, Y. Cao, Y. Chen, *Nat. Photonics* **2017**, *11*, 85.
[105] J. Yuan, J. Gu, G. Shi, J. Sun, H.-Q. Wang, W. Ma, *Sci. Rep.* **2016**, *6*, 26459.
[106] J. Yuan, M. J. Ford, Y. Xu, Y. Zhang, G. C. Bazan, W. Ma, *Adv. Energy Mater.* **2018**, *8*, 1703291.
[107] N. Li, C. J. Brabec, *Energy Environ. Sci.* **2015**, *8*, 2902.
[108] J. Hanisch, T. Wahl, C. D. Wessendorf, E. Ahlswede, *J. Mater. Chem. A* **2016**, *4*, 4771.
[109] L. Mao, J. Tong, S. Xiong, F. Jiang, F. Qin, W. Meng, B. Luo, Y. Liu, Z. Li, Y. Jiang, C. Fuentes-Hernandez, B. Kippelen, Y. Zhou, *J. Mater. Chem. A* **2017**, *5*, 3186.
[110] K. Glaser, P. Beu, D. Bahro, C. Sprau, A. Pütz, A. Colsmann, *J. Mater. Chem. A* **2018**, *6*, 9257.
[111] D. Angmo, T. R. Andersen, J. J. Bentzen, M. Helgesen, R. R. Søndergaard, M. Jørgensen, J. E. Carlé, E. Bundgaard, F. C. Krebs, *Adv. Funct. Mater.* **2015**, *25*, 4539.
[112] F. Guo, N. Li, V. V. Radmilović, V. R. Radmilović, M. Turbiez, E. Spiecker, K. Forberich, C. J. Brabec, *Energy Environ. Sci.* **2015**, *8*, 1690.
[113] A. R. bin Mohd Yusoff, D. Kim, F. K. Schneider, W. J. da Silva, J. Jang, *Energy Environ. Sci.* **2015**, *8*, 1523.
[114] J. Tong, S. Xiong, Z. Li, F. Jiang, L. Mao, W. Meng, Y. Zhou, *Appl. Phys. Lett.* **2015**, *106*, 053306.
[115] J. Tong, S. Xiong, Y. Zhou, L. Mao, X. Min, Z. Li, F. Jiang, W. Meng, F. Qin, T. Liu, R. Ge, C. Fuentes-Hernandez, B. Kippelen, Y. Zhou, *Mater. Horiz.* **2016**, *3*, 452.
[116] J. Adams, G. D. Spyropoulos, M. Salvador, N. Li, S. Strohm, L. Lucera, S. Langner, F. Machui, H. Zhang, T. Ameri, M. M. Voigt, F. C. Krebs, C. J. Brabec, *Energy Environ. Sci.* **2015**, *8*, 169.
[117] F. Livi, R. R. Søndergaard, T. R. Andersen, B. Roth, S. Gevorgyan, H. F. Dam, J. E. Carlé, M. Helgesen, G. D. Spyropoulos, J. Adams, T. Ameri, C. J. Brabec, M. Legros, N. Lemaitre, S. Berny, O. R. Lozman, S. Schumann, A. Scheel, P. Apilo, M. Vilkman, E. Bundgaard, F. C. Krebs, *Energy Technol.* **2015**, *3*, 423.
[118] N. Grossiord, J. M. Kroon, R. Andriessen, P. W. M. Blom, *Org. Electron.* **2012**, *13*, 432.
[119] P. Cheng, X. Zhan, *Chem. Soc. Rev.* **2016**, *45*, 2544.
[120] I. Fraga Domínguez, A. Distler, L. Lüer, *Adv. Energy Mater.* **2017**, *7*, 1601320.
[121] F. Bella, G. Griffini, J.-P. Correa-Baena, G. Saracco, M. Grätzel, A. Hagfeldt, S. Turri, C. Gerbaldi, *Science* **2016**, *354*, 203.
[122] Y. Lv, P. Xu, G. Ren, F. Chen, H. Nan, R. Liu, D. Wang, X. Tan, X. Liu, H. Zhang, Z.-K. Chen, *ACS Appl. Mater. Interfaces* **2018**, *10*, 23928.
[123] E. B. L. Pedersen, D. Angmo, H. F. Dam, K. T. S. Thydén, T. R. Andersen, E. T. B. Skjønsfjell, F. C. Krebs, M. Holler, A. Diaz, M. Guizar-Sicairos, D. W. Breiby, J. W. Andreasen, *Nanoscale* **2015**, *7*, 13765.
[124] H. F. Dam, T. R. Andersen, E. B. L. Pedersen, K. T. S. Thydén, M. Helgesen, J. E. Carlé, P. S. Jørgensen, J. Reinhardt, R. R. Søndergaard, M. Jørgensen, E. Bundgaard, F. C. Krebs, J. W. Andreasen, *Adv. Energy Mater.* **2015**, *5*, 1400736.
[125] T. T. Larsen-Olsen, T. R. Andersen, H. F. Dam, M. Jørgensen, F. C. Krebs, *Solar Energy Mater. Solar Cells* **2015**, *137*, 154.
[126] A. Brown, M. Green, *Prog. Photovoltaics* **2002**, *10*, 299.
[127] A. R. bin Mohd Yusoff, D. Kim, H. P. Kim, F. K. Shneider, W. J. da Silva, J. Jang, *Energy Environ. Sci.* **2015**, *8*, 303.
[128] Y. Gao, V. M. Le Corre, A. Gaïtis, M. Neophytou, M. A. Hamid, K. Takanabe, P. M. Beaujuge, *Adv. Mater.* **2016**, *28*, 3366.
[129] S. Esiner, R. E. M. Willems, A. Furlan, W. Li, M. M. Wienk, R. A. J. Janssen, *J. Mater. Chem. A* **2015**, *3*, 23936.
[130] X. Elias, Q. Liu, C. Gimbert-Suriñach, R. Matheu, P. Mantilla-Perez, A. Martinez-Otero, X. Sala, J. Martorell, A. Llobet, *ACS Catal.* **2016**, *6*, 3310.
[131] F. Guo, N. Li, F. W. Fecher, N. Gasparini, C. O. R. Quiroz, C. Bronnbauer, Y. Hou, V. V. Radmilović, V. R. Radmilović, E. Spiecker, K. Forberich, C. J. Brabec, *Nat. Commun.* **2015**, *6*, 7730.
[132] D. Bartesaghi, I. del Carmen Pérez, J. Kniepert, S. Roland, M. Turbiez, D. Neher, L. J. A. Koster, *Nat. Commun.* **2015**, *6*, 7083.
[133] R. Timmreck, T. Meyer, J. Gilot, H. Seifert, T. Mueller, A. Furlan, M. M. Wienk, D. Wynands, J. Hohl-Ebinger, W. Warta, R. A. J. Janssen, M. Riede, K. Leo, *Nat. Photonics* **2015**, *9*, 478.
[134] J. Gilot, M. M. Wienk, R. A. J. Janssen, *Adv. Funct. Mater.* **2010**, *20*, 3904.
[135] D. Bahro, M. Koppitz, A. Mertens, K. Glaser, J. Mescher, A. Colsmann, *Adv. Energy Mater.* **2015**, *5*, 1501019.
[136] D. Di Carlo Rasi, K. H. Hendriks, M. M. Wienk, R. A. J. Janssen, *Adv. Energy Mater.* **2017**, *7*, 1701664.
[137] M. Prosa, N. Li, N. Gasparini, M. Bolognesi, M. Seri, M. Muccini, C. J. Brabec, *Adv. Mater. Interfaces* **2017**, *4*, 1700776.
[138] S. Esiner, G. W. P. van Pruissen, M. M. Wienk, R. A. J. Janssen, *J. Mater. Chem. A* **2016**, *4*, 5107.
[139] G. Simone, D. Di Carlo Rasi, X. de Vries, G. H. L. Heintges, S. C. J. Meskers, R. A. J. Janssen, G. H. Gelinck, *Adv. Mater.* **2018**, *30*, 1804678.
[140] K. Mathieson, J. Loudin, G. Goetz, P. Huie, L. Wang, T. I. Kamins, L. Galambos, R. Smith, J. S. Harris, A. Sher, D. Palanker, *Nat. Photonics* **2012**, *6*, 391.